ISSN 1580-2949
UDK 669+666+678+53 MTAEC9, 41(4)155–195(2007)

MATER. TEHNOL.	LETNIK VOLUME 41	ŠTEV. NO. 4	STR. P. 155–195	LJUBLJANA SLOVENIJA	JULY-AUGUST 2007

VSEBINA – CONTENTS

UDC/UDK 539.4:620.17
Original scientific article/Izvirni znanstveni članek

ISSN 1580-2949
MTAEC9, 41(4)157(2007)

A FATIGUE CHARACTERIZATION OF HONEYCOMB SANDWICH PANELS WITH A DEFECT

UTRUJENOSTNA KARAKTERIZACIJA SATASTIH SENDVIČNIH PANELOV Z NAPAKO

Boualem Keskes[1,2] , Yves Menger[1], Ahmed Abbadi[1], Joseph Gilgert[1], Nourredine Bouaouadja[2] , Zitouni Azari[1]

[1]LFM Université de Metz ENIM Île du Saulcy, F-57045 Metz cedex 01, France
[2] Mechanic and Optic department, University of Setif Algeria, Algeria
b_keskes@univ-metz.fr

Prejem rokopisa – received: 2006-12-11; sprejem za objavo – accepted for publication: 2007-02-19

Honeycomb sandwich panels are used because of their high stiffness, good fatigue resistance and low weight. These panels are used in a variety of applications, but particularly in the aerospace industry. When this is the case a simple knowledge of the static properties is not sufficient and additional information about the fatigue properties is required. In real situations these panels can be affected by manufacturing defects and impacts, and it is important to know the effects of these defects and the behaviour of the damaged panel; it also important to determine the location of the defect. In our investigation these defects will be simulated by a blind hole in the centre of the lower face sheet. Static and fatigue tests (four-point bending) with acoustic-emission monitoring were carried out on sandwich panels with defects. The load/displacement and the *S-N* fatigue curves are presented and analyzed.

Key words: sandwich, honeycomb, four-point bending, fatigue, defect, acoustic emission

Satasti sendvični paneli se odlikujejo po veliki togosti, dobri odpornosti proti utrujenosti in nizkem razmerju mase. Te panele se uporablja za različne namene, posebno v letalski industriji. V tem primeru ni dovolj poznanje statičnih lastnosti, zato so potrebne dodatne informacije o utrujenosti. Pri uporabi lahko na lastnosti panelov vplivajo napake pri izdelavi in poškodbe, zato je treba poznati učinek napak in razvoj poškodb, pa tudi znati določiti mesto poškodbe. Napake so v tem delu simulirane s slepo izvrtino v sredini spodnje površine panelne plošče.

Izvršeni so bili statični in utrujenostni preizkusi s štiritočkovnim upogibom z akustično emisijo na panelih z napako. Predstavljene in analizirane so odvisnosti obremenitev – pomik in utrujenostne krivulje S-N.

Ključne besede: sendvič, satje, 4-točkovni upogib, utrujenost, napaka, akustična emisija

1 INTRODUCTION

The main benefits of using the sandwich concept in structural components are the high stiffness, the good fatigue resistance and the low weight. Recent advances in materials and manufacturing techniques have resulted in further improvements and the increased uniformity of the properties of sandwich composites. In order to use these materials in different applications, a knowledge of their static properties alone is not sufficient, and additional information about their fatigue properties is required. However, many difficulties are encountered, mainly in forecasting their fatigue life, which reduce the utilisation of such materials in various industrial and aerospace applications.

Investigations of the bending-fatigue behaviour of sandwich beams were performed by Olsson and Lönnö [1], Echtermeyer et al. [2], Allen and Shenoi [3], Lagunegrand et al. [4], Burman and Zenkert [5]. It was found that under fatigue cycling of constant amplitude, the nucleation phase of fatigue damage extends over the major part of the fatigue life, while the phase of defect propagation is very short. The fatigue life of a component will also be adversely affected by damage, though the magnitude of this reduction in fatigue life is often more difficult to establish [6,7]. The fatigue of damaged (initial defects) structures may be determined by the extensive testing of specimens with various defects at different load levels [8].

Static overload or fatigue damage may cause significant degradation of the core or skin, which is not easily detectable by a visual inspection or conventional non-destructive evaluation techniques. Damage in a sandwich structure is not only caused by in-service loads; in the manufacturing processes used, defects within the sandwich, such as skin/core interface disbanding and stress concentrations at joints between core materials, can also occur [9,10].

Acoustic emission (AE) provides the possibility to monitor, dynamically in real time, the response to a discontinuity under an imposed structural stress, and has a significant advantage over other non-destructive testing methods. AE is a quality-control and non-destructive evaluation (NDE) technique that has proven to be most useful in metals and sandwich-composite structures [11,12]. Basically, AE employs a transducer, fixed to the structure, which registers emitted sounds from the loaded structure. The emitted sounds are then quantified and compared to a database of known sound-defect relationships, and the degree of damage from which the sounds are emitted can be quantified [13]. The analysis of the AE signals in the time and frequency domains can allow AE monitoring to be used to identify failure modes.

Attempts to correlate our results with those from other researchers are also complicated by the effect that acquisition parameters, such as filtering, threshold settings and sensor response, may have on the processed results. Of primary interest when performing mechanical testing utilising AE equipment, is the amount of activity (e.g. hits, events or counts), when it occurs (relative to load and/or time), where it originates (multiple sensor arrays allow location detection), and the characteristics of the signals in both the time and frequency domains. The signal amplitude is widely used as the first stage of damage characterisation. The main disadvantage of AE is that it requires a knowledge of the signal-propagation characteristics and a history of typical failures for the material and the structure under investigation. In practice it is common to determine experimentally the velocity by measuring the time taken by a known signal to travel a defined distance. The sound velocity in the sandwich panel was found to be approximately 2500 m/s [12,14].

To establish a robust fatigue-life model, a better understanding of the various failure mechanisms during cyclic loading is necessary. Fatigue tests (four-point bending) have been carried out on sandwich panels with and without a defect. To study the growth of the damage near the hole, AE was used, since it was expected that the different stages of the failure mode would be revealed. The expected result is a diminution of the remaining fatigue-life time, in proportion to the size of the hole.

2 MATERIAL AND EXPERIMENTAL TECHNIQUES

Sandwich panels consist of an aluminium core and a pure aluminium face sheet. The honeycomb core is an open cell with a density of 82 kg/m^3 of aluminium core. The cell size is 9.6 mm. The dimensions of these panels are shown in **Table 1**.

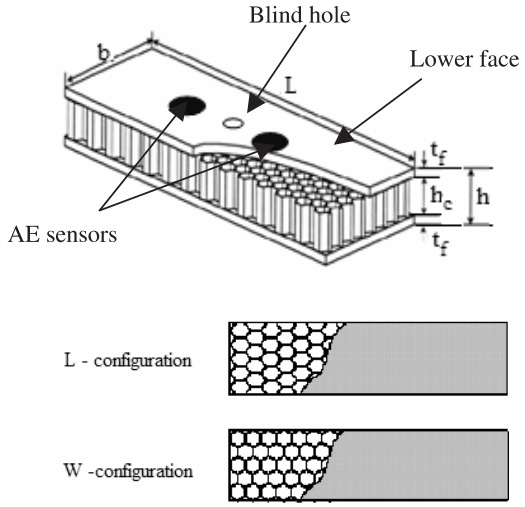

Figure 1: Honeycomb sandwich panel showing L and W configurations [15]
Slika1: Satasti sendivčni panel v L- in v W-konfiguraciji [15]

Table 1: Sample dimension
Tabela 1: Dimenzije preizkušanca

L (mm)	b mm	h mm	h_c (mm)	t_f mm	L_2 mm	L_1 mm
500	250	10	8.80	0.60	420	210

The skin material is $AlMg_3$ 5754. The properties of the core are shown in **Table 2** [15].

Table 2: Core mechanical properties
Tabela 2: Mehanske lastnosti jedra panela

Material	Aluminium – Aluminium
Core	ECM
Cell dimension /mm	6.4
Density /(kg/m^3)	82
Shearing Strength (configuration L) /MPa	2.4
Shearing Modulus (configuration L) /MPa	430
Shearing Strength (configuration W) /MPa	1.40
Shearing Modulus (configuration W) /MPa	220
Compression Strength /MPa	4.5

The beams with defects were tested with four-point bending and were monitored with AE, as shown in **Figures 1 and 2**. The tests were carried out with a servo-hydraulic Instron 8501 universal testing machine with a 10-KN capacity and a 2-mm/min crosshead velocity (**Figure 3**).

Cyclic flexural tests were also performed. The tests were carried out under load control at a load ratio R = 0.1 using a sinusoidal wave form. The beams were cycled at a frequency of 2 Hz. The fatigue data were generated at load levels of 100 %, 90 %, 80 %, 70 % and 60 % of the ultimate static load. The fatigue life of the specimens is defined as the number of cycles to ultimate failure. The normalised applied load is plotted against the number of cycles on a log-log scale.

The AE system used was a Vallens AMSY-5, data-acquisition unit with Vallens SE-45-type trans-

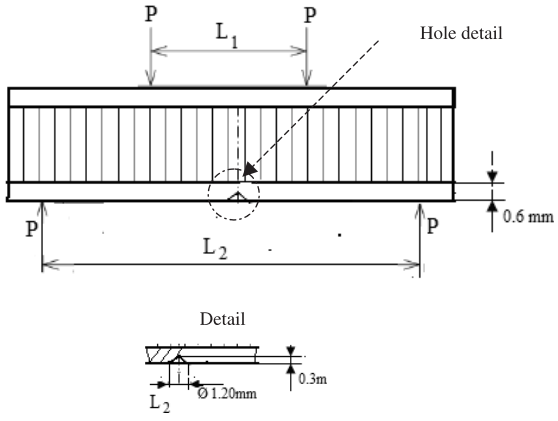

Figure 2: Schematic of sandwich beam for four-point bending and hole geometry
Slika2: Shema sendvične grede pri 4-točkovnem upogibu in geometrija izvrtine

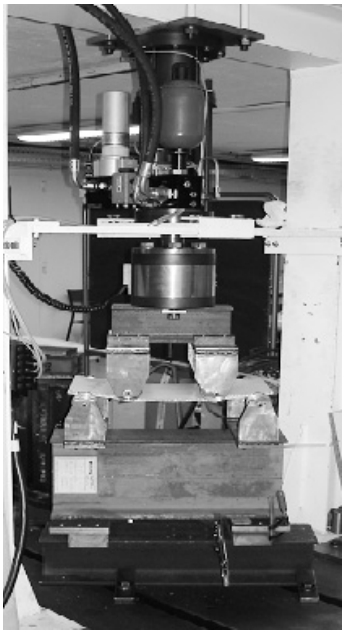

Figure 3: Test setup
Slika 3: Shema preizkusne naprave

ducers [16]. These sensors have sensitivity in the range 25 kHz to 120 kHz and a secondary range of sensitivity from 120 kHz to approximately 450 kHz. The AE signal was band-pass filtered with a 30 kHz to 1 MHz preamplifier and the total system amplification maintained at 40 dB allowed processing of the preamplifier input signal up to 99.9 dB above 1 mV (±99 mV peak). The AE sensors were mounted directly on the lower skin without any preparation of the contact surface using petroleum jelly as the acoustic coupling. The contact pressure was maintained with elastic tape.

3 RESULTS AND DISCUSSION

3.1 Static tests

AE was used to detect the damage and the crack mechanisms in the structure. **Figures 4 to 5** show the

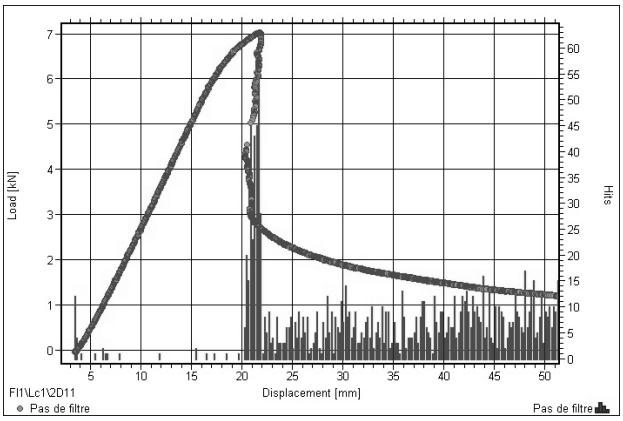

Figure 4: Load-deflexion Alu-Alu direction W
Slika 4: Obremenitev upogiba Alu-Alu v smeri W

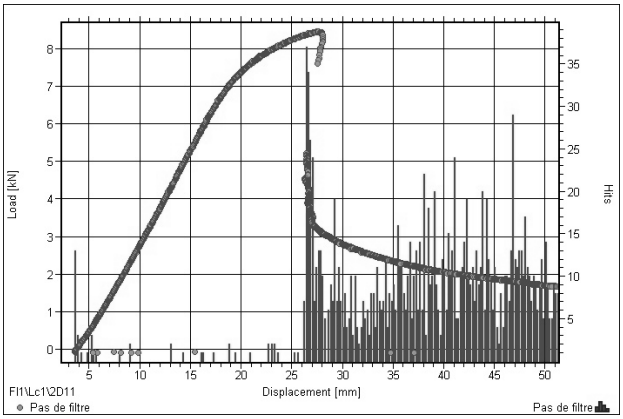

Figure 5: Load-deflexion Alu-Alu direction L
Slika 5: Obremenitev upogiba Alu-Alu v smeri L

applied load vs. the displacement. However, the same observation can be made with the energy or the amplitude of the events. The same test had already been performed on the same sample, but without a defect [10].

We observed that the sandwich structures present a maximum ultimate load and exhibit ductile behaviour. The material shows more resistance in the L than in the W cell configuration (**Figures 4 and 5**). At the beginning of the plasticity domain, and during the catastrophic failure, there is intense AE activity. Moreover, the hole does not have an influence on the static behaviour of the honeycomb sandwich panels. The modes of collapse were identified: the face yield, the cell buckling, and the indentation beneath the loading rollers, as shown in **Figure 6**.

These modes of collapse are confirmed by a number of investigations [6,8] The final failure for all the static tests occurred in the top skin and the core by a local indentation in the vicinity of the loading points, as illustrated in **Figure 6**. The localization of the damage in all cases was in the region close to the support, between the support and the adjacent load application.

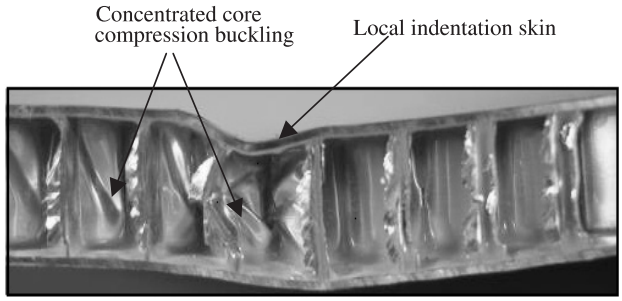

Figure 6: Failure mode showing local indentation skin and cell buckling
Slika 6: Način poškodbe z lokalnim vdorom in izločanjem aluminijastih celic

3.2 Fatigue tests

To investigate the effect of the defect (hole) on the fatigue life, flexural tests were performed in the cell direction L for an aluminium-aluminium sandwich panel with 82 kg/m^3.

Both curves (**Figures 7 and 8**) show the AE activity (Energy) vs. time and the minimal displacement vs. time. AE makes it possible to locate the crack initiation. Indeed, when the crack begins to grow there is a peak in the energy consumed. The displacement vs. time dependence shows that the crack initiation occurred at the same time.

The Wöhler curves were plotted with all the results of these tests and compared to the results for the same panels without a defect (**Figure 9**).

The results show that the fatigue life is the highest for the panels without a defect for the same applied load. Indeed, for an applied load of 65 % of the ultimate static load the number of cycles to failure is about of 5.10^5 cycles (**Figure 9**) for the panel with a defect, while for the panels without a defect it is greater than 10^6 cycles. The final fractures for the panels with and without a defect are shown in **Figure 10** and **Figure 11**, respectively. The crack started at the hole and grew in terms of its width (**Figure 10**).

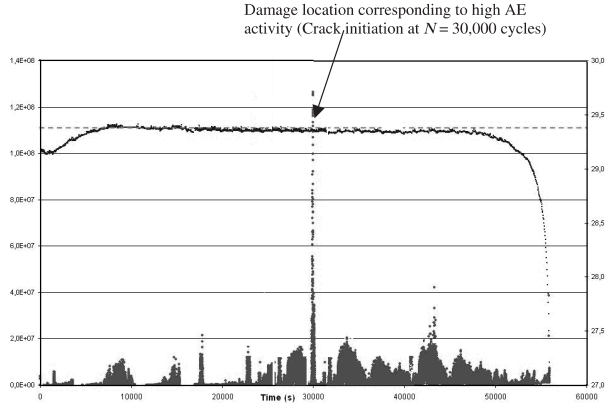

Figgure 7: Results for sample 1. AE activity (Energy) and the minimal displacement vs. time (80 % ultimate load)

Slika7: Primer AE aktivnosti za preizkušanec 1 in minimalen upogib v odvisnosti od časa (80 % končne obremenitve)

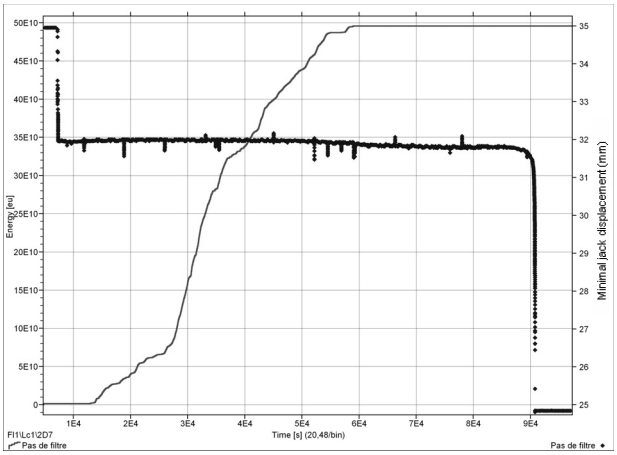

Figure 8: Results for sample 2. AE activity (Energy) and the minimal displacement vs. time (70 % ultimate load)

Slika8: Rezultati AE aktivnosti za preizkušanec 2 in minimalni upogib v odvisnosti od časa (70 % končne obremenitve)

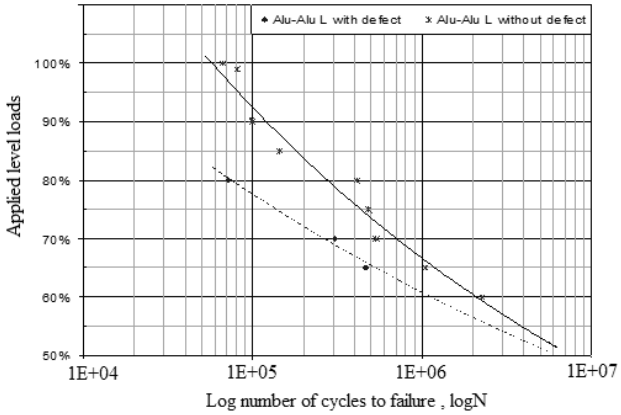

Figure 9: Wöhler Curves Aluminium-Aluminium

Slika 9: Wöhlerjeve krivulje aluminij-aluminij

4 CONCLUSION

Defect effects in static and fatigue studies of honeycomb core sandwich panels were investigated and the following observations were made.

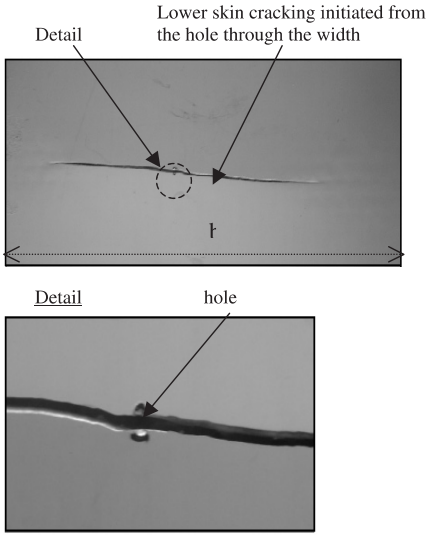

Figure 10: Fatigue-failure mode showing cracking skin through the defect

Slika 10: Utrujenostna poškodba, ki prikazuje razpoke skozi kožo

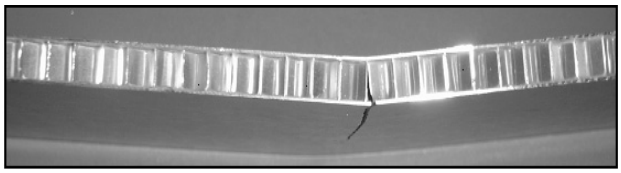

Figure 11: Fatigue-failure mode of the panel without a defect

Slika 11: Način preloma panela brez napake

No defect effect was observed in the case of the static study, in contrast to the case of the fatigue behaviour of the sandwich honeycomb panels. In the fatigue study, the fatigue life of the defect panels decreased rapidly when the applied load increased, compared to the panels without a defect. The results of the acoustic emission show the crack initiation and propagation and can be used as a reliable survey method for the damage mechanisms. The analysis of the acoustic signals confirmed that the majority of the damage growth occurs at peak-load levels and demonstrated the significant effect of the loading level on the progress of the damage.

5 REFERENCES

[1] Olsson KA, Lönnö A., Test procedures for foam core materials, In: Olsson KA, Reichard RP, editors. Proceedings of the First International Conference on Sandwich Constructions. Solihull, UK: EMAS, UK, 1989, 293–318

[2] Echtermeyer AT, Buene L, McGeorge D, Sund OE. Four point bend testing of GRP sandwich beams – Part 1. Der Norske veritas VR-91-P0013. 1991

[3] Allen HG, Shenoi RA. Flexural fatigue tests on sandwich structures, In: Weismann-Bermann D, Olsson KA, editors. Proceedings of the Second International Conference on Sandwich Constructions. Solihull, 1992, 499–517

[4] Lagunegrand L, Lorriot Th, Harry R, Wargnier H. Design of an improved four point bending test on a sandwich beam for free edge delamination studies, Composites: Part B 37 (**2006**), 127

[5] Burman M, Zenkert D. Fatigue of undamaged and damaged honeycomb sandwich beams. J Sandwich Struct Mater (**2000**) 2, 50–74

[6] Kapil Mohana, Yip Tick Hon, Sridhar Idapalapati, Hong Pheow Seow Failure of sandwich beams consisting of alumina face sheet and aluminum foam core in bending Materials Science and Engineering A 409 (**2005**), 292–30

[7] A. Abbadi, Z. Azari, S. Belouatar, J. Gilgert, S. Dominiack Static and fatigue characterization of honeycomb sandwich panels JNC14 *Compiègne*, French (**2005**)

[8] Demelio G, Genovese K, Pappalettere C, An experimental investigation of static and fatigue behaviour of sandwich composite panels, Composites B Eng 32 (**2001**) 4, 299–308

[9] H. Chen, R. Bai, Postbuckling behavior of face/core debonded composite sandwich plate considering matrix crack and contact effect, *Compos Struct* 57 (**2002**) 1, 305–313

[10] Arnaud pollien, Yves Conde, Laurent Pambaguiam, Andreas Mortensen, Graded open Cell aluminium foam core sandwich beams Materials Science and Engineering A 404 2005)

[11] S. Mechraoui, S. Benmedakhene, S. Amami, A. Laksimi – Damage crack analysis of glass/epoxy composite laminates by acoustic emission, JNC15, Compiègne (**2005**)

[12] B. SHAFIQ, A. QUISPITUPA – Fatigue characteristics of foam core sandwich composites International Journal of Fatigue, 28 (**2006**), 96–102

[13] Nondestructive Testing Handbook-Volume 5, Acoustic Emission, Testing, American Society for NDT 5asnt), 1987

[14] Prosser W, Advanced AE techniques in composite materials research, Journal of Acoustic Emission 14, (**1996**) 3/4, 1–11

[15] EURO-COMPOSITES, ECM-Honeycomb Technical Manuel, Eurocomposites S.A, Luxembourg, 1998

[16] Vallen System, www.vallen.de.com

UDC/UDK 539.4:669.14.018.298
Original scientific article/Izvirni znanstveni članek

ISSN 1580-2949
MTAEC9, 41(4)163(2007)

FATIGUE PROPERTIES OF A HIGH-STRENGTH-STEEL WELDED JOINT

UTRUJENOSTNE LASTNOSTI ZVARA VISOKOTRDNEGA JEKLA

Zijah Burzić[1], Vencislav Grabulov[1], Stojan Sedmak[2], Aleksander Sedmak[3]

[1]Military Technical Institute, Katanićeva 15, 11000 Beograd, Serbia & Montenegro
[2]Faculty of Technology and Metallurgy, Karnegijeva 4, 11000 Beograd, Serbia & Montenegro
[3]Faculty of Mechanical Engineering, Kraljice Marije 16, 11000 Beograd, Serbia & Montenegro
zijah_burzic@rvkds.net

Prejem rokopisa – received: 2006-05-17; sprejem za objavo – accepted for publication: 2007-03-09

In addition to the strength and toughness properties, the fatigue properties of welded joints are necessary for the design of high-strength steel structures exposed to variable loading. Wöhler curves were determined for smooth tensile specimens tested with variable loading. The fatigue behaviour of a welded joint can be improved by removing the overfill; however, the fatigue properties are still lower than the values for the parent metal. Tests with pre-cracked specimens have shown the difference in the fatigue-crack growth-rate properties to be less significant than other crack parameters.

Keywords: HSLA, welded joint, low-cycle fatigue, high-cycle fatigue, crack growth rate

Utrujenostne lastnosti so potrebne poleg trdnosti in žilavosti za načrtovanje struktur iz visokotrdnih jekel, ki prenašajo spremenljivo obremenitev. Wöhlerjeve krivulje so bile določene za gladke preizkušance in spremenljivo obremenitev. Utrujenostno vedenje zvarjenega spoja se lahko izboljša z odstranitvijo nadvišenja, vendar ostanejo utrujenostne lastnosti nižje kot pri osnovnem materialu. Preizkusi na vzorcih z razpoko so pokazali, da je manj izrazita razlika v hitrosti rasti razpoke kot pri drugih parametrih razpoke.

Ključne besede: HSLA, zvarjeni spoj, malociklična utrujenost, velikociklična utrujenost, hitrost rasti razpoke

1 INTRODUCTION

When selecting a material for a particular application, the ease and cost of welding must be considered, and the material selected should give a welded product with adequate properties for the minimum cost. The steels developed for heavily loaded structures and their welded joints have to be resistant to variable loading, in addition to having adequate strength and toughness properties [1]. The benefits of a strength increase can be expressed in terms of reduced component dimensions, followed by a significant reduction in welded-joint cross-sections, the consumption of welding electrodes and the time necessary to produce the welded joints.

Since defects are frequently involved in welded structures, it is necessary to design against low-stress failure by fatigue. By maintaining an adequate level of control by non-destructive testing, it is possible to ensure that cracks exceeding some maximum size, as the most dangerous defects, will be avoided and the stress concentration in components be reduced as a result. This is important for the welded joints of high-strength steel that are exposed to fatigue. The data about the fatigue behaviour of HSLA steel welded-joint constituents are necessary, starting with the design stage, since the benefits gained by having a high strength could be lost under variable loading.

2 PREPARATION OF SAMPLES

The experiments were performed with the high-strength steel NIONICRAL-70 (NN70), with the nominal yield-stress class of 700 MPa and its welded joints, produced with metal manual arc welding (MAW). This steel is designed for the manufacturing of pressure vessels and in shipbuilding, e.g., for submarines, but is also applicabble for other heavy-duty sructures. The chemical composition and the mechanical properties are shown in **Tables 1 and 2**, respectively.

Two plates of NIONICRAL-70, 18 mm thick, were prepared by edge machining for asymmetric 2/3 X and welded in 6 passes with a Tenacito-80 electrode, which produced a slightly undermatched welded joint.

3 TESTING FOR FATIGUE-ENDURANCE DETERMINATION

Low-cycle fatigue initiation can be expected in the region of welded joints, because the yield stress can be achieved locally by stress concentration. The smooth specimens for testing with variable loading are presented in **Figure 1**. Four sets of smooth specimens were prepared: OM, from the parent metal and from welded samples; XN, in the as-welded condition; XB, with the overfill removed by grinding; and XO, with both sides machined to 15 mm and so the rough layer of rolling was removed together with the overfill. The specimens were

Table 1: Chemical composition of NIONICRAL-70 steel, *w*/%
Tabela 1: Kemična sestava jekla Nionicral 70, *w*/%

C	Si	Mn	P	S	Cr	Ni	Mo	V	Al
0.1	0.2	0.23	0.009	0.018	1.24	3.1	0.29	0.05	0.08

Table 2: Mechanical properties of NIONICRAL-70 steel
Tabela 2. Mehanske lastnosti jekla Nionicral 70

Specimen orientation	Yield stress	Tensile strength	Elongation	Contraction	Charpy V impact energy, *E*/J		
	$R_{p0.2}$/MPa	R_m/MPa	*A*/%	Z/%	+20 °C	–60 °C	–100 °C
Parallel	780	820	19	66	126	117	93
Perpendicular	770	810	20	74	81	76	49

tested on a hydraulic machine, with the lower grip fixed and the upper grip oscillating with the frequency f = 9 Hz to 15 Hz, depending on the maximum load in the cycle, σ_g , at the stress ratio $R = \sigma_d/\sigma_g = 0.1$ (σ_d is the lower stress in the cycle). Local plastic deformation ahead the crack tip is typical for crack initiation and growth in the early stage of low-cycle fatigue, followed by shear lips. But, if the frequency is low, in low-cycle fatigue of high-strength steel the fracture appearance is similar to that obtained in high-cycle fatigue, with no shear lips. In some cases the loading level was so low that the specimens did not fracture, even after more than one million cycles. As a result of this they were tested in a high-cycle regime.

For a high stress level (691 MPa), close to the yield stress (**Table 2**), the as-welded XN specimens fractured with low-cycle fatigue after only 6700 cycles. The fatigue crack initiated in the region of stress concentration, in the transition from the overfill to the heat-affected zone (HAZ), and developed through the HAZ's coarse-grain region, followed by significant contraction of the cross-section. The crack grows on both sides of the specimen, and the final fracture occurred in the weld metal in a reduced ligament size. At a stress of 415 MPa the specimen fractured after 66,300 cycles. The high-cycle fatigue crack in the third XN specimen initiated in the same region and propagated in the plane normal to the load direction, completely through the HAZ's coarse-grain region of reduced ductility. The stress level was 274 MPa and the number of cycles at fracture was 143,700. The stress concentration in the XB specimens was reduced by removing the overfill. This increased the number of cycles to fracture: (a) for stress 685 MPa to 13,700 cycles, (b) for 228 MPa to 690,800 cycles. The crack initiated in the HAZ's coarse-grain region in both low-cycle (a) and high-cycle (b) fatigue and developed mostly through the HAZ. The best results for the welded samples were obtained with machined sides of the XO specimen in the absence of the stress concentration due to geometry. The crack initiated in the weld metal's critical microstructure. In low-cycle fatigue (a) the crack developed under 45° at a load of 586 MPa, up to 49,100 cycles. In high-cycle fatigue (b) the crack path is normal to the applied load of 443 MPa, and the fracture occurred after 565,300 cycles. In some specimens the crack initiated from embedded defects.

The results are summarized in the upper part of the relationship applied load σ vs. number of cycles N (Wöhler) (**Figure 2**). The fracture stress is satisfactory for the parent metal (OM) σ = 625 MPa and for the machined specimens (XO) σ = 530 MPa, but the results for the XN specimens in the as-welded condition (σ = 370 MPa) and for the XB specimens with the overfill

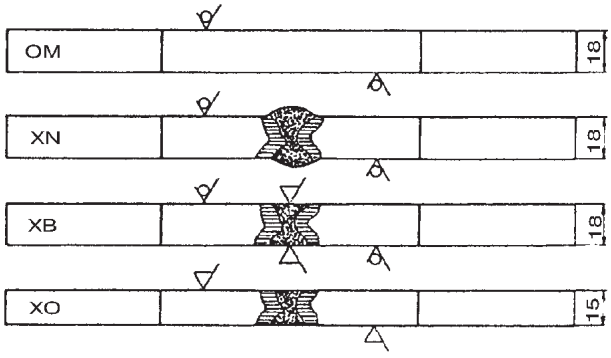

Figure 1: Smooth specimens for testing by variable loading
Slika 1: Gladki preizkušanci za preizkus pri variabilni obremenitvi

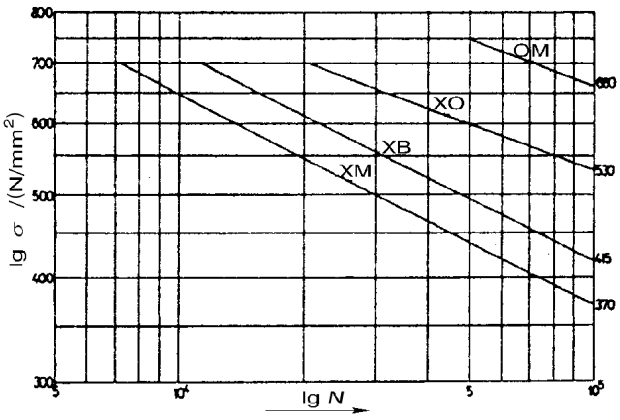

Figure 2: Upper part of the relationship applied load σ vs. number of cycles N
Slika 2: Zgornji del odvisnosti obremenitev – število amplitud

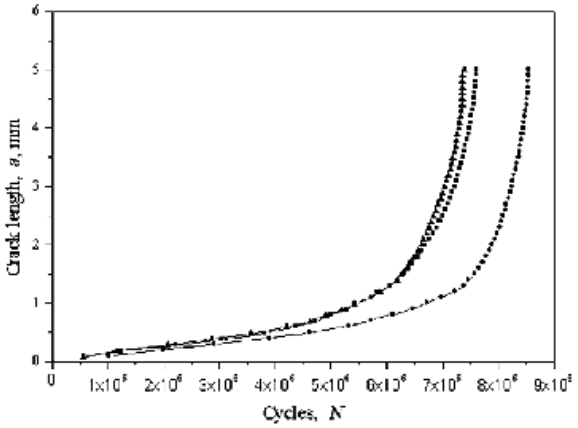

Figure 3: Crack length *a* vs. number of cycles *N* for parent metal (right), weld metal (in the middle) and HAZ (left)
Slika 3: Odvisnost dolžine razpoke – število ciklov za osnovni material (desno), deponirani material (sredina) in HAZ (levo)

ground away (σ = 415 MPa) are not acceptable. This is confirmed by the value of the coefficient *m* – the Wöhler curve slope in the initial part, up to 100,000 cycles, which is 5.90 for the OM specimens, 5.80 for the XO specimens, 4.23 for the XB specimens and 4.17 for the XN specimens. The recommended design values are 5 to 7 [2].

4 TESTING OF FATIGUE-CRACK GROWTH RATE

Welded structures can contain small pre-existing cracks, which will propagate under repeated loads up to the size critical for fracture. Since in this case the zone ahead of the crack tip, exposed to the cyclic plasticity, is small, a plane-strain state is formed, even for a small thickness, and generally the data obtained with small specimens can be applied.

The testing of the fatigue-crack growth rate is performed using the ratio R = 0.1, with precracked SE(B) specimens (width W = 16 mm, thickness B = 12 mm, span $S = 4W$) of parent metal, weld metal and HAZ, on a CRACKTRONIC dynamic testing device. The number of cycles was registered for each 0.1 mm of crack growth, as presented in the crack length *a* vs. number of cycles of *N* relation (**Figure 3**). The curve on the right-hand side is for the parent metal, the middle

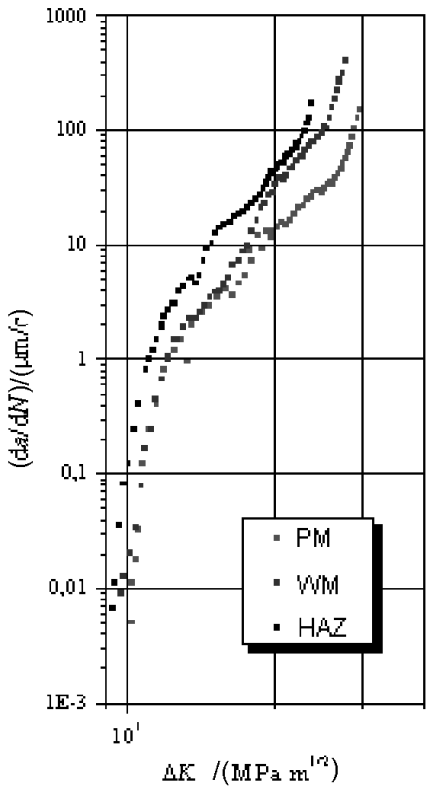

Figure 4: Diagram d*a*/d*N* – Δ*K*
Slika 4: Odvisnost d*a*/d*N*-Δ*K*

curve is for the weld metal, and the curve on the left-hand side is for the HAZ. From these curves the data necessary for Paris law are derived:

$$\frac{\mathrm{d}a}{\mathrm{d}N} = C(\Delta K)^{\mathrm{m}} \qquad (1)$$

Here, d*a*/d*N* is the crack size *a* growth per unit cycle, *N* is the cycle number, *C* and *m* are constants obtained from experiments and given in **Table 3**, $\Delta K = K_{max} - K_{min}$ is the stress-intensity factor range in the loading cycle.

The obtained relationships d*a*/d*N* vs. Δ*K* are given in **Figure 4**. It is interesting that the difference in the fatigue threshold value, the value of the stress-intensity factor range, ΔK_{th}, at which existing crack will not grow, is not significant: for the parent metal it is 10.22 MPa $m^{1/2}$, for the weld metal it is 9.11 MPa $m^{1/2}$ and for heat-affected zone it is 8.51 MPa $m^{1/2}$.

Table 3: The values for parameters *C* and *m* in the Paris equation
Tabela 3: Vrednosti parametrov *C* in *m* v Parisovi enačbi

Specimen	*C*	*m*	Specimen	*C*	*m*
Parent metal			HAZ		
I	$3.98 \cdot 10^{-14}$	4.139	I	$1.90 \cdot 10^{-20}$	10.259
II	$1.67 \cdot 10^{-13}$	3.765	II	$4.63 \cdot 10^{-12}$	2.667
Weld metal			III	$2.90 \cdot 10^{-16}$	6.403
I	$8.38 \cdot 10^{-15}$	4.798	IV	$7.87 \cdot 10^{-13}$	3.560
II	$3.30 \cdot 10^{-19}$	8.462	V	$1.48 \cdot 10^{-16}$	6.505
III	$7.93 \cdot 10^{-15}$	5.078	VI	$1.74 \cdot 10^{-14}$	4.929

5 CONCLUSIONS

The importance of reducing the stress concentration for fatigue life can be easily seen from **Figure 3**. The critical load for $N = 10^5$ cycles for the smooth parent-metal specimen is 625 MPa, reduced in the machined specimen of the welded joint to 530 MPa, with the overfill ground away it is reduced to 415 MPa, and down to 370 MPa in the as-welded condition.

In regime I the crack-growth rate is low since the threshold for the crack ΔK_{th} is approached. In regime II the Paris law is obeyed, while in regime III the crack-growth rate increases above that predicted by the Paris relation.

The fatigue resistance of the weld metal and the HAZ is reduced, compared to the parent metal, and this has to be taken into account when a welded structure is designed with high-strength steel.

Acknowledgement

The paper was prepared with the financial support of the Serbian Ministry of Science and Environment Protection – project ON 14027 "Special topics in fracture mechanics of materials".

6 REFERENCES

[1] W. S. Pellini: Guidelines for fracture-safe and fatigue-reliable design of steel structures, The Welding Institute, Abington, Cambridge, 1983

[2] H. W. Munse: Fatigue of welded steel structures, Welding Research Council, 1964

UDK/UDC 669.14:620.17:621.791.05
Izvirni znanstveni članek/Original scientific article

ISSN 1580-2949
MTAEC9, 41(4)167(2007)

MEHANSKE LASTNOSTI ZVARA IZ JEKLA MARAGING PO IZLOČEVALNEM ŽARJENJU

MECHANICAL PROPERTIES OF MARAGING STEEL WELDS AFTER AGING HEAT TREATMENT

Damjan Klobčar, Janez Tušek

Fakulteta za strojništvo, Univerza v Ljubljani, Aškerčeva 6, 1000 Ljubljana, Slovenija

Prejem rokopisa – received: 2006-09-21; sprejem za objavo – accepted for publication: 2007-06-06

V industriji tlačnega litja aluminija so bile narejene pilotne raziskave, ki naj bi potrdile mnenje, da orodja iz jekel maraging dosežejo daljšo trajnostno dobo in s tem nižjo ceno ulitka. Zato smo se odločili, da jekla maraging uporabimo za reparaturno varjenje orodij. Ta raziskava je del tiste, s katero smo ugotavljali primernost tega jekla za reparaturno varjenje orodij za tlačno litje aluminija. Cilj dela je bil ugotoviti optimalne parametre izločevalnega žarjenja varov iz jekla maraging, ki bodo zagotovili optimalne mehanske lastnosti. Posebej pripravljene varjence z utori v obliki črke U smo po postopku TIG navarili z jeklom maraging UTP A702. Varjenje je potekalo z minimalnim vnosom energije v zaščitni atmosferi plina argona. Tako pripravljene varjence smo izločevalno žarili pri časih od 0,7 h do 10,8 h ter temperaturah od 445 °C do 515 °C. Analizirali smo tudi varjence v navarjenem stanju in tiste, katerih varki so bili med varjenjem kovani. Iz posameznega varjenca smo izdelali 3 epruvete ISO-V za žilavost, rezino za analizo mikrostrukture in trdote ter 7 miniaturnih epruvet za natezno trdnost. Navar iz jekla maraging doseže optimalne mehanske lastnosti z 2-urnim izločevalnim žarjenjem na temperaturi 480 °C. Izločevalno žarjenje pri temperaturi 515 °C naj bi trajalo 1 h, pri temperaturi 445 °C pa 3 h. Kovanje varkov povečuje žilavost zvara.

Ključne besede: jeklo maraging, izločevalno žarjenje, mehanske lastnosti, mikrostruktura, varjenje TIG, tlačno litje aluminija

Investigations have shown that tools from maraging steels achieved longer tool life in high pressure die casting of aluminum. We have decided to check the use of maraging steel for repair welding of tools. A part of more extensive investigation aimed to establish the suitability of maraging steel for repair welding of high pressure die-casting toolings is done. In this work the results of the investigation used to establish optimal precipitation hardening parameters of maraging steel welds, which provides optimal mechanical properties is presented. Specimens with a "U" shaped grove were weld cladded with maraging steel UTP A702. GTA welding was carried out in protective atmosphere of argon gas and with minimal heat input. The test specimens were than precipitation annealed from 0.7 h to 10.8 h and temperatures from 445 °C to 515 °C. Specimens in as-welded condition and specimens with hammered welds were checked parallely. From same specimen 3 ISO-V specimens for toughness test, a slice for microstructure analysis and measurement of hardness, and 7 miniature specimens for tensile test were manufactured. The results showed that maraging steel welds achieve optimal mechanical properties after precipitation annealing for 2.5 h at 480 °C. Precipitation annealing at 515 °C should last for 1 h and at 445 °C for 3 h. The hammering of welds increases weld toughness.

Keywords: maraging steel, precipitation annealing, mechanical properties, microstructure, GTA welding, high pressure die-casting, response surface modelling

1 UVOD

Tlačno litje aluminijevih zlitin je velikoserijski postopek za proizvodnjo izdelkov zahtevnih geometrijskih oblik v ozkih dimenzijskih tolerancah. Med tlačnim litjem se v orodje vliva talino aluminijeve zlitine s temperaturami do 700 °C, pri čemer je hitrost taline od 30 m/s do 100 m/s ter polnilni tlak od 50 MPa do 80 MPa [1]. Te obremenitve krajšajo trajnostno dobo orodij s a) termičnimi cikli, ki povzročajo utrujenostne razpoke na površini gravure, b) s korozijo ali sprijemanjem taline aluminija na gravuro, c) z erozijo površine zaradi pretoka aluminija in č) lomom orodja [2-4]. Končna cena ulitka je odvisna od parametrov tlačnega litja, ki vplivajo na trajnostno dobo orodja. Namen raziskave je podaljšati trajnostno dobo orodij za tlačno litje aluminija z reparaturnim varjenjem, pri čemer bi kot dodajni material uporabili jekla maraging zaradi njihovih izjemnih mehanskih lastnosti.

Prednost jekel maraging v primerjavi s klasičnimi za delo v vročem se kaže v manjšem modulu elastičnosti in manjšem linearnem temperaturnem razteznostnem koeficientu (**tabela 1**). To povzroča manjše napetosti v orodju med temperaturnimi obremenitvami. Večja toplotna prevodnost jekla maraging dodatno zmanjša temperaturo površine in posledično napetosti. Maraging jekla imajo v primerjavi s klasičnimi jekli za delo v vročem večjo žilavost in trdnostne lastnosti, kar vpliva na boljšo odpornost proti termičnemu utrujanju. Za uspešno podaljšanje trajnostne dobe orodja morajo imeti materiali za orodja za tlačno litje aluminija dobro stabilnost mehanskih lastnosti pri povišanih temperaturah. To dosegajo z jekli maraging z vsebnostjo niklja 14 % [5], 12 % (Thyrotherm 1.2799) ali celo 2 % [6]. Manjša vsebnost Ni premakne transformacijo ferita v avstenit k višjim temperaturam. Slabost manjše vsebnosti Ni je slabša žilavost [6].

Nasprotno od klasičnih orodnih jekel za delo v vročem imajo jekla maraging omejeno vsebnost C, H in N, svoje odlične lastnosti pa dosežejo z legiranjem s/z Co, Mo, Ti in Al [7-9]. Dodatna prednost je njihova odlična varivost, saj jih pri varjenju ni treba predgrevati ali

Tabela 1: Mehanske in fizikalne lastnosti jekel [5,12]
Table 1: Mechanical and physical properties of steels [5,12]

Lastnost	1.2344	UTP A702 1.6356	Marlok C1650
Gostota /(kg/dm^3)	7,8	–	8,09
Modul elastičnosti /GPa	210	191	186
Natezna trdnost /MPa	1430	1763	1600
Meja plastičnosti /MPa	1230	1688	1500
Trdota /HRc	43–54	40–50	47–51
Žilavost /J			
20 °C	15–20	15–21	25
200 °C	–	–	35
400 °C	–	–	45
Temperaturni koeficient dolžinskega raztezka /(10^{-6} mm/(mm °C))			
20°C–400°C	12,5	–	10
20°C–600°C	13,1	–	5,6
Toplotna prevodnost /(W/(m °C))			
20 °C	25	–	28
500 °C	28,5	–	32
600 °C	29,3	–	33

Tabela 2: Kemična sestava jekel v masnih deležih (%) [5,12]
Table 2: Chemical composition of steels in % [5,12]

Element	1.2344	1.6356	Marlok C1650
C	0,3–0,4	0,02	<0,008
Cr	4,8–5,5	–	<0,30
Mo	1,2–1,5	4,0	4,5
Ni	–	18,0	14,0
Co	–	12,0	10,5
Ti	–	1,6	0,2
Si	0,8–1,2	–	<0,10
Mn	0,2–0,4	–	<0,10
Al	–	0,1	–

pogrevati, da bi dobili duktilen in žilav martenzit. Tudi mehanska in EDM-obdelava se izvajata laže kot pri klasičnih orodnih jeklih.

Toplotna obdelava jekla maraging zajema topilno in izločevalno žarjenje. Topilno žarjenje poteka pri temperaturah 815–915 °C eno uro, pri tem pa se v avstenitu topijo legirni elementi. Po ohlajanju na zraku se tvori mehak martenzit, nasičen z legirnimi elementi. Pri varjenju z manjšim vnosom energije kot 1,8 kJ/mm topilno žarjenje ni potrebno in varjenju sledi izločevalno žarjenje [10]. Slednje navadno poteka pri temperaturah od 470 °C do 550 °C približno tri ure, dejanski parametri pa so odvisni od kemične sestave jekla. Med tem žarjenjem se v materialu tvorijo izločki, ki povzročajo deformacije kristalnih rešetk. To povzroča linearno spremembo dimenzij od 0,05 % do –0,1 %, velikost spremembe pa je odvisna od parametrov izločevalnega žarjenja [8].

Kljub odličnim mehanskim lastnostim se jekla maraging le malo uporabljajo kot material za orodja. Vzrok je višja cena. Naša ideja je bila, da bi uporabili jekla maraging za reparaturno popravilo orodij oz. za navarjanje na površino. S tem bi dobili cenovno sprejemljiva visokokakovostna orodja. Na površino orodja za tlačno litje aluminija je treba navariti dovolj debelo plast jekla maraging, da preprečimo akumulacijo toplote na prehodu med osnovnim jeklom in navarjeno plastjo. Uspešen odvod energije s površine orodja bomo zagotovili, če bo površinski sloj jekla maraging segal do hladilnih kanalov.

Namen študije je bil karakterizirati jekla maraging (z 18 % Ni) glede na mehanske lastnosti in mikrostrukturo. Narejena je bila analiza varjenja TIG jekla maraging glede na vnos energije, temperaturo predgrevanja in kovanje varkov, analiziran pa je bil tudi vpliv parametrov izločevalnega žarjenja na razvoj mikrostrukture in mehanske lastnosti.

2 EKSPERIMENTALNI DEL

Pripravljena je bila serija vzorcev iz jekla 1.2344 z izdelanim utorom U po **sliki 1**. Pred navarjanjem so bili vzorci poboljšani na trdoto *HRc* 46. V posamezen utor U je bilo po postopku TIG navarjenih 14 varkov, dolgih 75 mm. Varjenje je potekalo z varilnim tokom 150 A, varilno napetostjo 12 V, s hitrostjo varjenja 5 cm/min in vnosom energije 2,1 kJ/mm v zaščiti plina argona s pretokom 10 L/min. Navarjali smo dodajni material jeklo maraging 1.6356 (**tabela 2**), ki je bilo v obliki palic premera 2,5 mm in dolžine 1000 mm. Tik pred varjenjem smo s površine varilnih žic odbrusili bakreno zaščitno plast ter žico očistili z acetonom. S tem smo preprečili kontaminacijo vara z bakrom. Teme varka smo pred varjenjem novega varka očistili z žično ščetko in acetonom. Varjenje večine vzorcev je potekalo pri temperaturi predgrevanja 100 °C, en vzorec je bil varjen s predgrevanjem pri temperaturi 400 °C, varki enega vzorca pa so bili med varjenjem ročno kovani. S kovanjem spremenimo natezne zaostale napetosti v zvaru v tlačne in zmanjšamo verjetnost pokanja med termičnim utrujanjem.

Navarjeni vzorci so bili izločevalno žarjeni po načrtu izločevalnega žarjenja, ki je bil izdelan s statističnim načrtovanjem eksperimentov. Uporabili smo središčno zasnovan načrt eksperimentov in metodologijo površin odziva, ki omogoča razvoj regresijskih modelov višjega reda. Parametri izločevalnega žarjenja so bili določeni tako, da zajamejo širše območje toplotne obdelave.

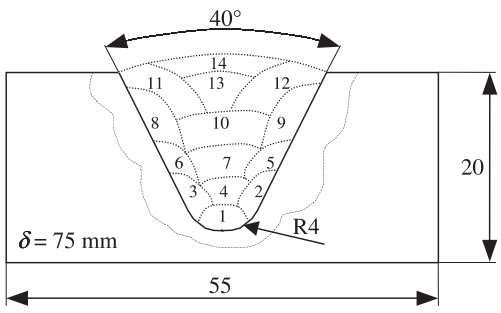

Slika 1: Shema gradnje varkov v vzorcu z utorom U
Figure 1: Schematic of U grove specimen weld filling

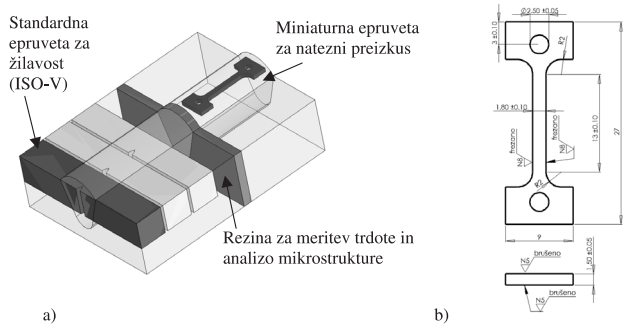

Slika 2: Iz varjenca smo izrezali: a) 7 miniaturnih epruvet za natezni preizkus, 3 standardne epruvete ISO-V za žilavost ter rezino za meritev trdote in analizo mikrostrukture. b) Shematičen prikaz epruvete za natezni preizkus.

Figure 2: From the welded specimen were manufactured: a) 7 tensile test specimens, 3 toughness test specimens and a slice for microstructure analysis. b) Scheme of tensile test specimen.

Temperatura izločevalnega žarjenja je bila izbrana v območju od 445 °C do 515 °C, čas pa v območju od 0,7 h do 10,8 h. Centralna točka središčno zasnovanega načrta eksperimentov je bila izbrana po priporočilu proizvajalca pri 480 °C in treh urah.

Varjenci so bili po varjenju in toplotni obdelavi razrezani po shemi na **sliki 2**. Iz vsakega varjenca so bile izdelane tri epruvete ISO-V za preizkus žilavosti, rezina za analizo mikrostrukture in sedem miniaturnih epruvet za natezni preizkus. Natezni preizkusi so bili narejeni na računalniško krmiljeni napravi Zwick Z050, ki je imela vgrajen senzor sile GTM 50 kN in ekstenziometer tip 66607. Preizkusi so bili izvedeni po standardu EN 10002-1. Preizkus udarne žilavosti po Charpiju je bil opravljen v skladu s standardoma EN 10045-1:2000 in EN 10045-2:1992. Iz posameznega varjenca so bile preizkušene tri epruvete ISO-V in izračunane povprečne vrednosti žilavosti.

Na rezinah vzorcev je bila narejena metalografska analiza in meritev trdote po Vickersu. Vzorci so bili polirani in jedkani v 4-odstotni raztopini nitala (4 % HNO_3 + 96 % C_2H_5OH) ter pregledani na optičnem mikroskopu.

3 REZULTATI

Diagram na **sliki 3** prikazuje trdoto in natezno trdnost temenskih varkov iz jekla maraging v navarjenem stanju ter žilavost večvarkovnega vara iz jekla maraging. Najvišjo natezno trdnost 1170 MPa je dosegel var, narejen pri temperaturi predgrevanja 100 °C. Kovan varek je imel nekoliko nižjo natezno trdnost (1046 MPa), medtem ko se je pri varku, narejenem pri temperaturi predgrevanja 400 °C, drastično zmanjšala natezna trdnost na 953 MPa. Trdota temenskega vara v navarjenem stanju je bila *HV* 400, kar je več kot trdota jekla maraging v homogeniziranem stanju, ki ima od *HV* 305 do *HV* 339. Trdota se je pri tem povišala zaradi izločevalnega žarjenja med varjenjem TIG ter zaradi temperature predgrevanja. Trdota kovanih varkov se je zvišala na *HV* 410 zaradi kovanja, ki varke mehansko utrdi. Trdota temenskega varka, narejena pri temperaturi predgrevanja 400 °C je bila *HV* 390. Padec trdote je posledica večjega vnosa energije med varjenjem, ki se pojavi zaradi višje temperature predgrevanja. Največjo žilavost zvara ˜ 86 J smo dobili pri varjencu s kovanimi varki. Žilavost vara v navarjenem stanju je bila 80 J, medtem ko je bila žilavost vara, narejena pri temperaturi predgrevanja 400 °C, le 56 J.

Slika 4 prikazuje potek trdote in natezne trdnosti temenskih varkov iz jekla maraging ter žilavost večvarkovnega vara v navarjenem stanju in po izločevalnem žarjenju z različnimi parametri. Iz diagrama je razvidno, da se z višanjem temperature in daljšanjem časa izločevalnega žarjenja natezna trdnost in trdota povečujeta, medtem ko se žilavost zmanjšuje. Občuten padec žilavosti se pojavi že po kratkotrajnem izločevalnem žarjenju (480 °C/ 0,7 h), ko se v mehkem martenzitu oblikujejo izločki, mikrostruktura pa je še premalo starana (**slika 5a**). Pri tem doseže var žilavost 27,7 J, trdoto *HV* 410 in natezno trdnost 1306 MPa. S povečanjem temperature in časa izločevalnega žarjenja dobimo dobro staran var, katerega mikrostruktura je prikazana na **sliki 5b** (445 °C/ 3 h). Za dobro staran var je značilna žilavost okoli 20 J, trdota okoli *HV* 505 ter natezna trdnost 1383 MPa. Če čas izločevalnega žarjenja

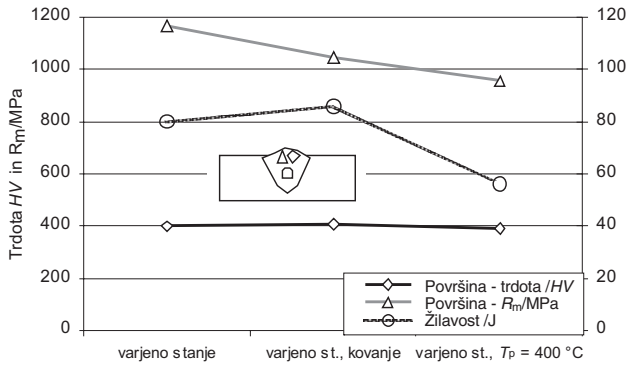

Slika 3: Trdota, žilavost in natezna trdnost temenskih varov v varjenem stanju v odvisnosti od tehnologije varjenja

Figure 3: Hardness, toughness and tensile strength of surfacing weld in as-welded condition of different conditions welding

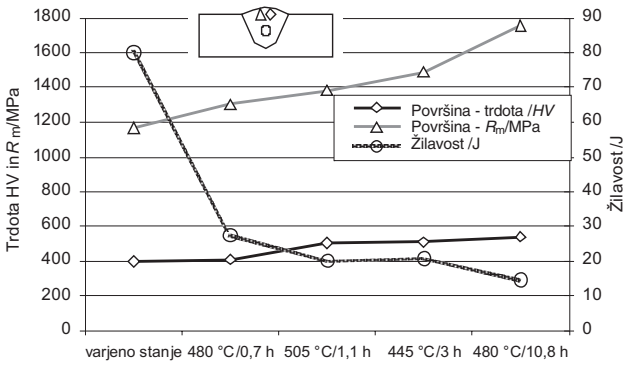

Slika 4: Trdota, žilavost in natezna trdnost varov v varjenem stanju ter po izločevalnem žarjenju z različnimi parametri

Figure 4: Hardness, toughness and tensile strength of a surfacing weld after different precipitation hardening

še podaljšamo in/ali povišamo temperaturo (npr. 480 °C/ 10,8 h), dobimo preveč starano mikrostrukturo (**slika 5c**). Zanjo je značilna trdota *HV* 540, natezna trdnost 1758 MPa in žilavost 14,6 J.

Pri izbiri parametrov toplotne obdelave izločevalnega žarjenja je potrebna posebna pozornost. Izbrati je namreč treba parametre, ki dajo najbolj ustrezne mehanske lastnosti za posamezno aplikacijo. S tem namenom je bila narejena statistična analiza mehanskih lastnosti varov iz jekla maraging z metodologijo površin odziva. Izdelani so bili modeli za napoved trdote, žilavosti in natezne trdnosti v odvisnosti od parametrov izločevalnega žarjenja. Modeli so prikazani v grafični obliki na **slikah 6a–c**). Povečanje temperature in/ali časa toplotne obdelave izločevalnega žarjenja poveča trdoto in natezno trdnost ter zmanjša žilavost vara iz jekla maraging.

Mikrostrukture varov so primerjane na **sliki 5**. Mikrostruktura na **sliki 5a** je premalo starana in je tipična za var v varjenem stanju oz. za var, izločevalno žarjen pri prekratkih časih ali prenizkih temperaturah. Mikrostruktura, prikazana na **sliki 5b**, je dobro starana in

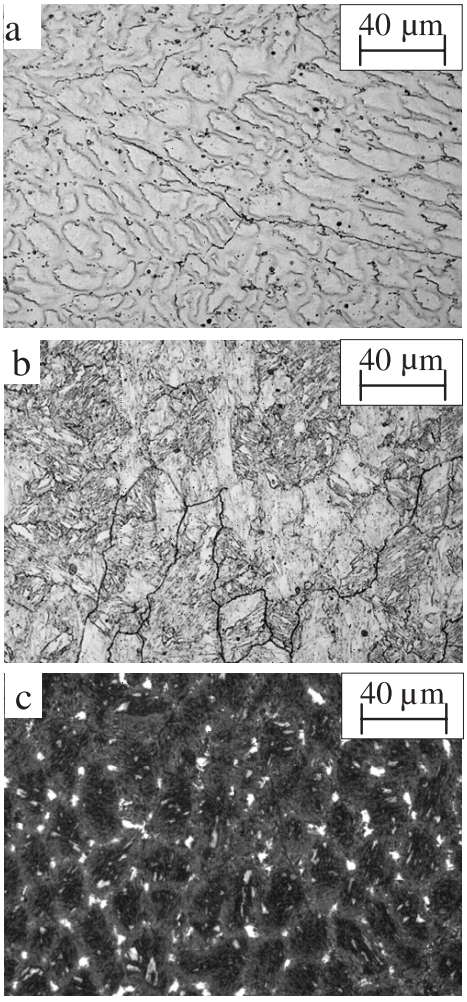

Slika 5: Mikrostrukture temenskih varkov po izločevalnem žarjenju: a) 480 °C / 0,7 h, b) 445 °C / 3 h, 480 °C / 10,8 h

Figure 5: Microstructures of surfacing welds after precipitation hardening: a) 480 °C / 0,7 h, b) 445 °C / 3 h, 480 °C / 10,8 h

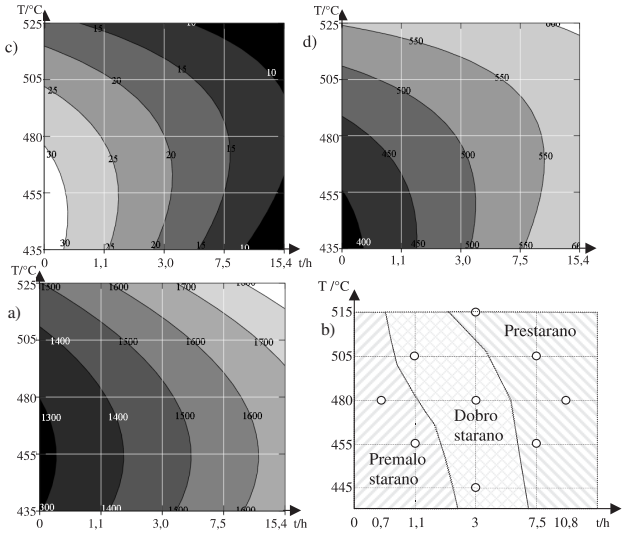

Slika 6: Spreminjanje a) žilavosti /J, b) trdote *HV*, c) natezne trdnosti /MPa in d) stanja mikrostrukture v odvisnosti od parametrov izločevalnega žarjenja

Figure 6: Change of weld a) toughness, b) hardness, c) tensile strength and d) microstructure after different precipitation annealing

jo dobimo pri izločevalnem žarjenju z optimalnimi parametri. **Slika 5c** je značilna za preveč starano mikrostrukturo. Na mejah med celičnimi dendriti se pojavijo značilna bela področja, ki so bogata z Ni. Na teh mestih se pretvorba v povratni avstenit pojavi že pri nižjih temperaturah. Taka mikrostruktura ni želena, ker ima majhno žilavost. Pri bolj izrazitem prestaranju se znižata tudi trdota in natezna trdnost, kar posledično vpliva na večjo obrabo in slabšo odpornost proti termičnemu utrujanju.

Na osnovi analize mikrostrukture je bil izdelan grafični prikaz stanja mikrostrukture glede na parametre izločevalnega žarjenja (**slika 6d**). Premalo staran var dobimo pri izločevalnem žarjenju pri nižjih temperaturah krajši čas. Dobro staran var dobimo z izločevalnim žarjenjem s parametri iz osrednjega področja, preveč staran var pa z izločevalnim žarjenjem pri visokih temperaturah in dolgih časih. S **slike 6d**) lahko ugotovimo take parametre izločevalnega žarjenja, pri katerih bomo v izbranem jeklu dobili želeno mikrostrukturo. Če te rezultate kombiniramo z razvitimi modeli za napoved mehanskih lastnosti, dobimo dodatno informacijo, ki omogoča lažjo izbiro parametrov izločevalnega žarjenja za aplikacijo.

4 DISKUSIJA

Priporočen vnos energije med varjenjem je po literaturi 1,8 kJ/mm [10], mi pa smo varili z vnosom energije 2,1 kJ/mm. Mikrostruktura vara v navarjenem stanju je premalo starana in ima visoko žilavost ter relativno nizko trdoto in natezno trdnost. Glede na trdoto jekla maraging v homogeniziranem stanju je trdota v navarjenem stanju večja. Zaradi manjšega povečanja trdote in premalo starane mikrostrukture topilno žarjenje ni

potrebno. Kljub temu pomeni varjenje z vnosom energije 2,1 kJ/mm zgornjo vrednost vnosa energije.

Kovanje varkov med varjenjem je zamudno. Pri varjenju trdih in krhkih orodij je pogosto neizogibno, da preprečimo pokanje. Kovanje spremeni natezne zaostale napetosti, ki nastanejo v varu zaradi varjenja, v tlačne in posledično preprečuje širjenje razpok. Varom iz jekla maraging poveča žilavost in trdoto. Višja žilavost je najverjetneje posledica drobljenja večjih kristalnih zrn v manjša, višja trdota pa je posledica mehanske utrditve. Kovanje varkov iz jekla maraging je priporočljivo.

Predgrevanje na temperaturo 400 °C negativno vpliva na mehanske lastnosti vara iz jekla maraging, saj zmanjšuje trdoto, natezno trdnost in žilavost, najverjetneje zaradi segrevanja varkov v območju temperatur od 700 °C do 1000 °C, to je v območju krhkosti. Pri tem se na mejah avstenitnih zrn in celičnih dendritov pojavijo Ti(C, N)-izločki, ki povzročajo krhkost jekla [7]. Zaradi pomanjkanja Ti v preostanku mikrostrukture sta manjša tudi natezna trdnost in trdota zvara. Predgrevanje na temperaturo 400 °C se zato ne priporoča. Najvišja temperatura predgrevanja, ki jo priporoča literatura, je 200 °C [12]. Jekla maraging so dobro variva tudi pri sobni temperaturi, ker se pri ohlajanju na zraku pojavi duktilen in žilav martenzit.

Povečanje trdote in natezne trdnosti ter zmanjšanje žilavosti s povečevanjem časa in temperature izločevalnega žarjenja je že poznano iz literature. Pri tem je zanimivo, da se povečanje trdote in natezne trdnosti sklada s padcem žilavosti. To je v skladu z objavljenimi podatki v literaturi za jekla maraging [8,12]. Pri tem velja poudariti, da literatura navadno ne navaja podatkov za natezno trdnost, niti podatkov za mehanske lastnosti zvarov. Prednost razvitih modelov za napoved mehanskih lastnosti po izločevalnem žarjenju je, da lahko parametre določimo na osnovi želenih mehanskih lastnosti. S tem zagotovimo, da ima material optimalne mehanske lastnosti za določeno uporabo že vnaprej in posledično vplivamo na trajnostno dobo orodja.

Grafičen prikaz stanja mikrostrukture varov iz jekla maraging glede na parametre izločevalnega žarjenja predstavlja pomembno informacijo pri izbiri optimalnih parametrov za posamezno aplikacijo. Če ta model kombiniramo z modeli za napoved mehanskih lastnosti ter z zahtevami orodjarjev, se nam zožijo možnosti izbire parametrov izločevalnega žarjenja. Kljub temu pa lahko izberemo take parametre, ki bodo omogočali višjo trdoto ali natezno trdnost ali višjo žilavost.

5 SKLEPI

Analiza varjenja TIG jekla maraging z 18 % Ni ter analiza izločevalnega žarjenja varov glede na mikrostrukturo in mehanske lastnosti je pokazala naslednje:

- varjenje z vnosom energije do 2,1 kJ/mm je praktično in povzroča le delno izločevalno žarjenje vara, zato topilno žarjenje po varjenju ni potrebno;
- temperatura predgrevanja 400 °C je previsoka za varjenje jekel maraging z vsebnostjo 18 % Ni ali več. Priporoča se predgrevanje do 200 °C;
- kovanje varkov je zaželeno, saj zvišuje žilavost in trdoto varkov ter spreminja natezne zaostale napetosti v tlačne;
- izločevalno žarjenje poteka hitreje pri višjih temperaturah. S povečevanjem temperature in časa izločevalnega žarjenja se natezna trdnost in trdota povečujeta, žilavost pa pada;
- dobro starano mikrostrukturo dobimo npr.: pri izločevalnem žarjenju na temperaturi 515 °C eno uro, pri temperaturi 445 °C tri ure oz. z uporabo razvitih modelov, ki so prikazani na **sliki 6**;
- premalo starano jeklo maraging ni primerno za površinski sloj orodij, ker ima prenizko trdoto, pri preveč staranem materialu pa se pojavi občuten padec žilavosti.

6 LITERATURA

[1] A. Srivastava, V. Joshi, R. Shivpuri, Computer modeling and prediction of thermal fatigue cracking in die-casting tooling, Wear 256 (**2004**), 38–43

[2] A. Persson, S. Hogmark, J. Bergstrom, Simulation and evaluation of thermal fatigue cracking of hot work tool steels, International Journal of Fatigue 26 (**2004**), 1095–1107

[3] A. Persson, S. Hogmark, J. Bergstrom, Thermal fatigue cracking of surface engineered hot work tool steels, Surface and Coatings Technology 191 (**2005**), 216–227

[4] W. Young, Why Die Casting Dies Fail, Paper No. G-T79-092, 10th SDCE International die casting exposition & congress, St.Louis, Missouri, North American Die Casting Association, 1979

[5] Metso Powdermet, Materials Technology Solutions, Marlok, Longer die life Better quality, www.metsopowdermet.com/, (2005)

[6] Y. Wang, A study of PVD coatings and die materials for extended die-casting die life, Surface and Coatings Technology 94–95 (**1997**), 60–63

[7] R. F. Decker, S. Floreen, Maraging steels – The first 30 years, Wilson, R. K., Maraging steels – recent developments and applications, The Metals & Minerals Society, Warrendale, PA, 1988

[8] J. Grum and M. Zupančič, Suitability assessment of replacement of conventional hot-working steels with maraging steel, Part I: Mechanical properties of maraging steel after precipitation hardening treatmen, Zeitschrift fuer Metallkunde/Materials Research and Advanced Techniques 93 (**2002**), 164–170

[9] J. Grum, M. Zupančič, Suitability assessment of replacement of conventional hot-working steels with maraging steel, Part II: Microstructure of maraging steel after precipitation hardening treatment, Zeitschrift fuer Metallkunde/Materials Research and Advanced Techniques 93 (**2002**), 171–176

[10] D. A. Canonico, Gas Metal-Arc Welding of 18 % Nickel Maraging Steel, Welding Research (**1964**), 433–442

[11] D. Klobčar, J. Tušek, B. Taljat, G. Scavino, Influence of thermal fatique on materials for die-casting tooling, Rosso, M., Actis Grande, M., in Ugues, D., Tooling materials and their applications from research to market: proceedings of 7th International Tooling Conference, 2.5.2006 Torino, Politechnico di Torino, 479–485

[12] A. T. Minotto, B. Taljat, J. Tušek, Development of weld-cladding processes for surface enhancement of hot-work tooling, 5th International Conference on Industrial Tools, ICIT 2005, 12.4.2005 Velenje, TECOS Celje, 207–214

UDC/UDK 539.42:621.791.05
Original scientific article/Izvirni znanstveni članek

ISSN 1580-2949
MTAEC9, 41(4)173(2007)

AN EXPERIMENTAL VERIFICATION OF NUMERICAL MODELS FOR THE FRACTURE AND FATIGUE OF WELDED STRUCTURES

EKSPERIMENTALNA VERIFIKACIJA NUMERIČNIH MODELOV ZA PRELOM IN UTRUJENOST ZVARJENIH STRUKTUR

Stojan Sedmak[1], Aleksander Sedmak[2], Miodrag Arsić[3], Jelena Vojvodič Tuma[4]

[1]Faculty of Technology and Metallurgy, Karnegijeva 4, 11000 Beograd, Serbia & Montenegro
[2]Faculty of Mechanical Engineering, Kraljice Marije 16, 11000 Beograd, Serbia & Montenegro
[3]Institute for Material Testing, Bulevar vojvode Mišića 43, 11000 Beograd, Serbia & Montenegro
[4]Institute of Metals and Technology, Lepi pot 11, 10000 Ljubljana, Slovenia

Prejem rokopisa – received: 2006-05-17; sprejem za objavo – accepted for publication: 2006-12-19

By allowing a more detailed analysis, numerical modelling has an important role to play in the development of structures. However, the results of a numerical model's analysis have to be verified with an experimental analysis for the application. Two full-scale welded-structure tests were used for the verification of the proposed numerical models. In the first case a pressure vessel pre-cracked in weld metal and instrumented for a *J*-integral measurement was tested. In this way the crack's driving force, expressed as the *J* integral, could be determined directly. The crack's driving force was calculated by applying the Ratwani-Erdogan-Irwin (REI) numerical model. The experimental results were compared to the values obtained with the REI model. In was shown that the application of the model produces conservative results and that the model can be applied for a structural integrity assessment of cracked pressure vessels. The second case was the welded structure of a rotor excavator. The critical welded components were modelled in full scale. The loading was recorded with strain gauges at critical locations, analyzed and elaborated in the form of the stress spectrum applied in the testing. The experimental results were compared to those obtained with numerical models. The comparison revealed that the model significantly overestimates the real cycle number for the fatigue limit. These two examples clearly demonstrated the complexity of the problem. In the case of the pressure vessel the model results are conservative, while those obtained for the fatigue are too optimistic.

Keywords: welded joint, numerical model, experiment, fracture, fatigue

Numerično modeliranje je zelo pomembno za razvoj struktur, ker omogoča bolj natančno analizo, vendar je potrebno rezultate numerične analize eksperimentalno verificirati. Dve varjeni strukturi sta bili uporabljeni za verifikacijo predloženih numeričnih modelov. V prvem primeru je bila preverjena posoda pod pritiskom z razpoko v zvaru. Posoda je bila instrumentirana za neposredno določitev *J*-integrala. Gonilna sila za propagacijo razpoke je bila izračunana z numeričnim Ratwani-Erdogan-Irwinovim (REI) modelom. Eksperimentalne rezultate smo primerjali z REI-vrednostmi. Pokazalo se je, da so rezultati modela konservativni pri oceni integritete v primeru razpoke v posodi pod pritiskom. Drugi analiziran primer je bila zvarjena struktura dela rovokopača. Kritični zvarjeni del je bil modeliran v pravi velikosti. Obremenitev je bila registrirana z merilnimi trakovi na različnih mestih, nato pa analizirana in predstavljena v obliki spektra napetosti. Rezultati preizkusa so bili primerjani z rezultati iz numeričnega modela. Primerjava je pokazala, da model pomembno preceni realno število obremenitev do utrujenostne trdnosti. Ta dva primera kažeta na kompleksnost problema. V primeru posode pod pritiskom so rezultati modela konservativni, v primeru utrujenosti pa optimistični.

Ključne besede: zvarni spoj, numerični model, preizkus, prelom, utrujenost

1 INTRODUCTION

The impressive developments in fracture mechanics and the numerical modelling of structures during the past 40 years has enabled the improvement of existing and the introduction of new methods for the evaluation of residual life and the assessment of structural integrity [1]. By applying these methods the service safety of structures has been increased and their life has been extended, resulting in significant cost savings. Today, numerical modelling is an invaluable tool for the design of different structures, as well as the manufacturing and use of steel structures, power and petrochemical plants, aircraft, machinery and vehicles. Welded structures have a very important role in many of these sectors and, therefore, require special attention. The reason for this is the possibility of cracks occurring in welded joints, which can endanger the structural integrity and negatively affect the service safety. Many standards and documents consider this structural integrity, and probably the most important is the SINTAP (Structural INTegrity Assessment Procedure) [2,3], which is based on fracture-mechanics analyses and experience with cracks in a welded structure [4]. The fracture-mechanics approach was applied with success and formally accepted in the case of the Trans Alaska Crude Oil Pipeline [5], for a "fitness-for-purpose" approach. The maximum allowed crack size was verified experimentally before the proposal for when and how to repair the cracks in welded joints. The most important conclusion in this investigation was that "fracture-mechanics analysis is an acceptable basis for an allowable exception from valid standards under circumstances, under the condition that this analysis provides a clear and conservative structural integrity assessment".

Numerical models are developed based on the available data, which do not necessarily coincide in all cases with the real situation. Two important requirements before the acceptance of a proposed model are:

1. the model has to be conservative in order to cover different circumstances,
2. the model must be experimentally verified.

Experiments with full-scale welded structures are not frequently performed, because they are connected with many problems in their organization and realisation, and, not surprisingly, they are very expensive. The obtained results are, however, generally valid for the tested structure and the applied testing conditions. For this reason, numerical modelling has an important role to play in the development of structures since it allows a more detailed analysis. In any case, it is questionable whether the results of the numerical model analysis represent the real situation of the considered structure, because a large number of influential parameters have to be considered. The answer to this question can only be obtained from a proper experimental analysis.

2 CRACK-GROWTH ANALYSIS WITH THE J-INTEGRAL

Two aspects of the J integral have to be considered for a structural integrity assessment. In the first the J integral is an elastic-plastic fracture-mechanics parameter that defines the cracked body's geometry and the loading (the crack driving force – *CDF*), and in the second it represents the crack resistance of the material (J_{Ic} and *J–R* curve) [6]. The fundamental difference between these two aspects is the crack-growth behaviour. In the first case the crack size is not variable and it is used as a parameter with the stress. In the second case, however, the crack growth is included. The criterion for the initiation of stable crack growth is mathematically defined as:

$$J(\sigma, a) \geq J_{Ic} \tag{1}$$

where $J(\sigma,a)$ is the crack driving force (*CDF*), depending on the remote stress, σ, and the crack length, a, whereas J_{Ic} is the material's resistance to the initiation of stable crack growth. In the case of elastic-plastic fracture mechanics the crack growth analysis is not restricted to the application of Equation (1), but also involves the stable crack growth and the condition for the initiation of its unstable spreading, e.g., the *J–R* curve, which is compared to the *CDF* using a convenient graphical method. The initiation of unstable crack growth is given by:

$$\frac{\partial J(\sigma, a)}{\partial a} \geq \frac{\partial J}{\partial a} \tag{2}$$

indicating that the increase in the *CDF* must be greater than the increase of the material's crack resistance for the same crack extension. When the value $J(\sigma,a)$ reaches the value J_{Ic} (1), (the intersection of the *CDF* curve and the *J–R* curve), the stable crack growth is initiated, and it continues up to the instant at which $\partial J(\sigma,a)/\partial a$ becomes greater than $\partial J/\partial a$ (2), (the tangent of the *CDF* curve to the *J–R* curve) producing unstable crack growth. The extent of the stable crack growth, Δa, is the difference (on the abscissa) of the marked points A and a_o, including the crack-tip blunting.

A theoretical–analytical model, such as the Ratwani-Erdogan-Irwin (REI) model [7], can be applied for the *CDF* determination. The crack resistance can be determined experimentally, e.g., according to ASTM E1820 [8] or by applying the J-integral direct-measurement method [9].

3 VERIFICATION OF THE STRUCTURAL INTEGRITY ASSESSMENT MODEL

The conservative prediction of the structural integrity of a cracked welded structure means that the material's crack resistance is greater than the maximum *CDF*. Thus, it should be proved that the applied model for the *CDF* and the residual strength prediction is conservative. With this aim the experimental pressure vessel (**Figure 1**) was welded from high-strength low-alloyed SM80P steel (700 MPa yield strength class) 16-mm steel plates, applying a qualified welding procedure, and prepared for

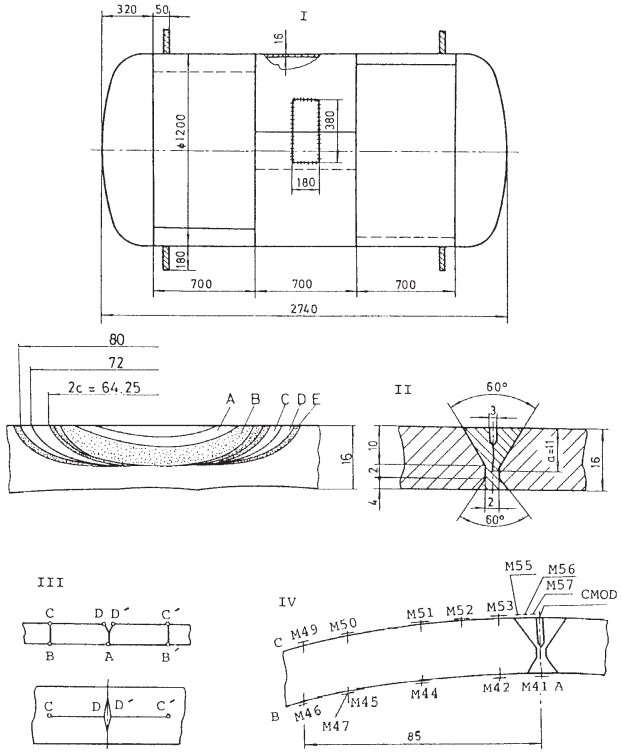

Figure 1: Experimental pressure vessel: I, shape and dimensions; II, detail of crack; III, integration path; IV, distribution of strain gauges. A notch. B fatigue pre-crack. C,D stable crack growth. E final fatigue

Slika 1: Eksperimentalna posoda pod pritiskom: I oblika in mere. II Detail razpoke. III pot integracije. IV Porazdelitev merilnih trakov za napetost. A zareza. B utrujenostna pred-razpoka. C, D Stabilna rast razpoke. E Končna utrujenost

the verification of the REI model [10]. This was performed using a J-integral direct measurement [9] on the fatigue pre-crack positioned in the WM (**Figure 1.II**). To prepare the fatigue pre-crack, a segment of size 180 mm × 380 mm, containing the SAW weld metal, was cut from the welded prototype. After machining the notch in the centre of the weld metal, a fatigue pre-crack was produced according to the standard procedure, and the segment was than re-welded in the pressure vessel. The properly selected contour DCBAB'C'D", given in **Figure 1.III**, was covered by regularly distributed strain gauges, **Figure 1.IV,** and the clip gauge applied for the crack-opening displacement enabled a direct evaluation of the *J* integral. It is interesting to note that during the test the crack increased in length, from the initial value of $2c$ = 64.25 mm up to 72 mm after the first stage and up to the final value of 80 mm measured after the experiment. The crack did not grow in terms of depth, as can also be seen in **Figure 1.II**.

The shell parameter λ, necessary in the next calculation for the crack length $2c$ = 64.25 mm for the mid-thickness shell radius $2R$ = 1184 mm, the wall thickness W = 16 mm, and the Poisson's ratio ν = 0.3, is:

$$\lambda = \left[12(1-\nu^2)\right]^{1/4} = \left[12(1-0.3^2)\right]^{1/4} \frac{32.125}{\sqrt{1184 \cdot 0.016}} = 0.6 \quad (3)$$

The crack driving forces for the axial surface crack in the pressure vessel were calculated using the REI model for this value of the shell parameter and expressed by the set of lines in **Figure 2**, depending on crack ratio, *a/W,* and the normalized pressures $pR/WR_{p0.2}$ (p is the applied pressure, $R_{p0.2}$ is the weld metal's yield stress). Point "A" is experimentally obtained at a pressure of 100 bar for the crack depth, measured after testing (a = 11 mm, crack ratio a/W = 0.69). For the same pressure CDF, calculated with the REI model for a/W = 0.69, is 40 %

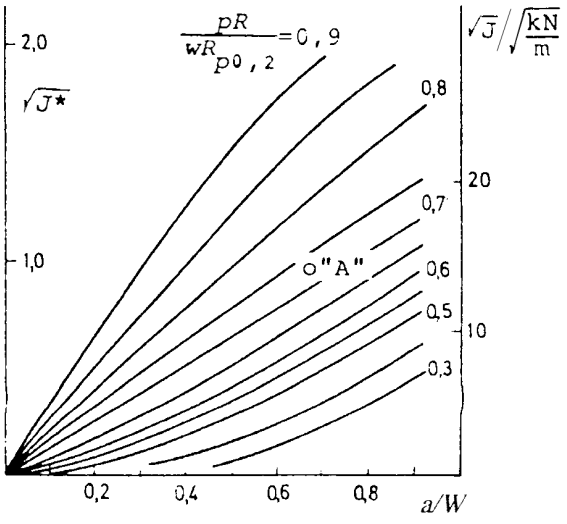

Figure 2: Crack driving forces with marked point "A" for the experimentally obtained *J* integral

Slika 2: Gonilna sila razpoke s točko A za eksperimentalno določen *J*-integral

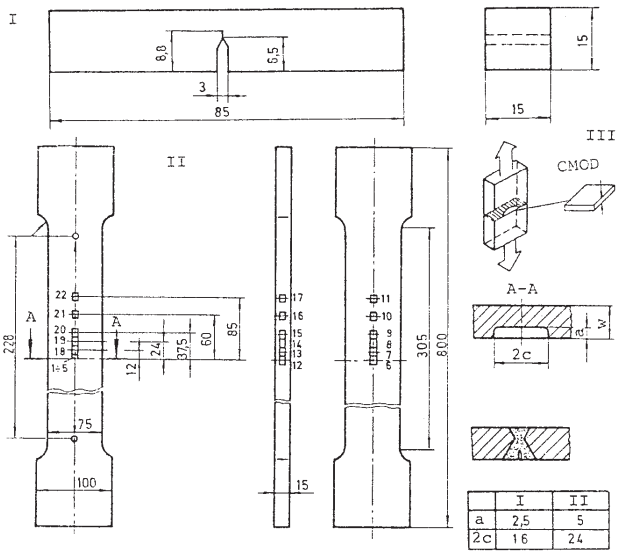

Figure 3: Pre-cracked specimens (I – three-point bend specimen; II – tensile panel, III – details of surface cracks on tensile panels)

Slika 3: Preizkušanci s pred-razpoko (I – tritočkovni upogibni preizkušanec; II – natezna plošča; III – detalj; s površinskimi razpokami na nateznih ploščah)

higher than the point "*A*", indicating that the model is conservative and can be used for a structural integrity assessment.

For the *J-R* curve the determination of the SEN (B) specimen was selected (**Figure 3.I**) for the single-specimen technique (ASTM E1820), and instrumented tensile panels with a surface crack (**Figure 3.II**) for the

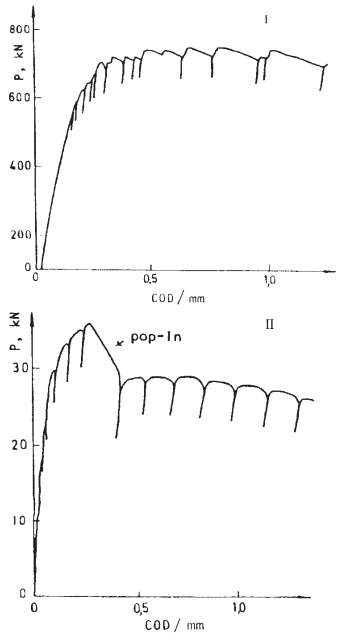

Figure 4. Typical plots of load, *P,* vs. crack-opening displacement (*COD*) for a crack in the HAZ (I – tensile panel; II – three-point bend specimen – arrow indicates "pop-in")

Slika 4. Tipične odvisnosti *P* od premika odprtja razpoke (*COD*) za razpoko v HAZ (I – natezna plošča; II – tritočkovni upogibni preizkušanec; puščica je označba točke "pop-in")

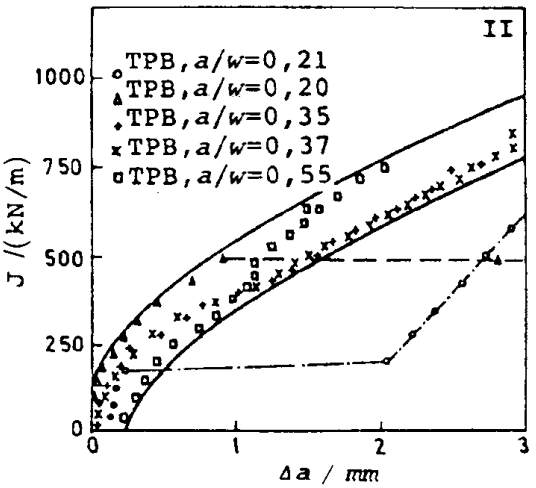

Figure 5: Scatter band *J–R* curves set of SEN(B) – TPB specimens for HAZ with two cases of pop-ins for *a/W* values 0.21 and 0.20

Slika 5: Trosenje območja krivulj *J–R* za SEN(B) – TPB-preizkušance za HAZ z dvema primeroma "pop-in" za vrednosti *a/W* 0,21 in 0,20

J-integral direct-measurement method [9]. The cracks located in the HAZ of the tensile panel are presented in **Figure 3.III**.

From the extended experimental program [10] the specimens precracked in the HAZ were selected as the most critical for the structural integrity assessment. The two plots of load vs. crack opening displacement are typical, one of the uniform form (tensile panels) and the other with "pop-in", indicating an arrested, rapidly growing crack (some of the SEN(B) specimens) (**Figure 4.II**). The derived corresponding *J-R* curves with critical SEN(B) specimens are presented in **Figure 5**.

The pop-in occurred only for the small ratio *a/W* = 0.21 and *a/W* = 0.20 in SEN(B) – TPB specimens of HAZ (**Figures 4 and 5**) indicating that a through crack can develop easily, which was not observed for tensile panels. In a real pressure vessel the crack is similar to that in the tensile panel and pop-in is not expected. The lower bound (LB) curve covers the pop-ins found during testing (**Figure 6**) and the obtained relations indicated that the structural integrity was not critical because of the crack ratio *a/W* = 0.548, the crack depth is a_o = 8.77 mm, the pressure of *p* = 120 bar, significantly higher than the operating pressure, can produce an unstable crack growth of an additional 0.8 mm, before the crack tip reaches the region of tougher material in which the crack can continue to grow under increasing pressure in a stable manner. A crack of that size is not probable in a real pressure vessel because much smaller cracks can be detected with non-destructive testing.

Thus, the structural integrity assessment of the cracked pressure vessel with the considered REI model is conservative and can be reliably applied.

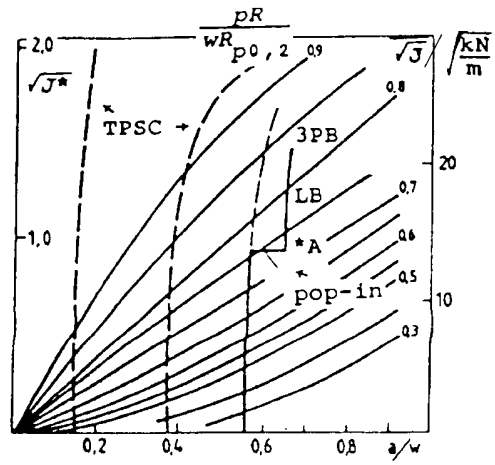

Figure 6: Structural integrity assessment for HAZ *J–R* curves lower bound (LB), including specimens with pop-in

Slika 6: Ocena integritete strukture za HAZ *J–R*-krivulje spodnjega praga (LB) z vključenim "pop-in"

4 VERIFICATION OF THE FATIGUE-CRACK GROWTH MODEL

Service fatigue cracks frequently occur in the welded components of rotor excavator bearing structures (**Figure 7**). The program of the performed investigation included the identification of critical regions, the measuring of strains with strain gauges in different service conditions, the determination of the stress spectrum, the model design of a critical welded joint and the model testing by constant amplitude load and using a defined stress spectrum. The obtained experimental results are compared to numerical solutions obtained by applying the linear fatigue-damage accumulation hypothesis by Palmgren-Miner [11], and a modified linear hypothesis, Corten-Dolan [12], Serensen-Kogaev [13] and Haibach [14].

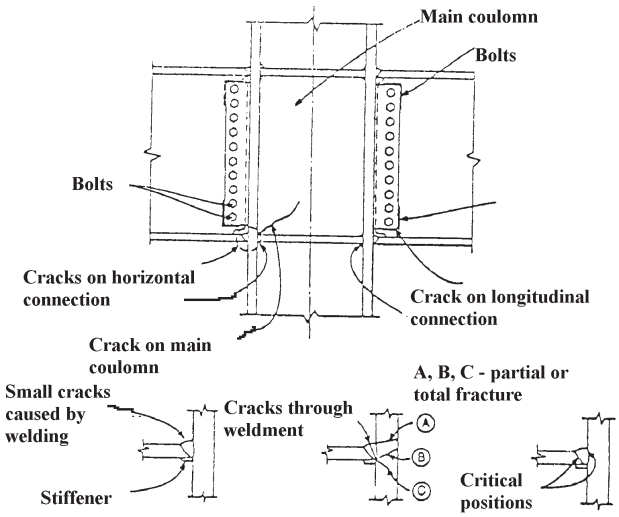

Figure 7: Cracks in critical regions of the welded components of a rotor excavator

Slika 7: Razpoke v kritičnih področjih zvarjenih komponent rotorja rovokopača

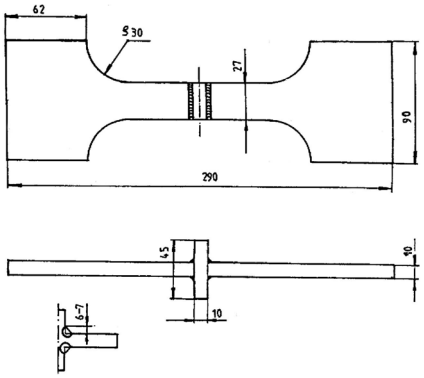

Figure 8: Specimen for fatigue testing, model of cross-welded joint of rotor excavator arrow

Slika 8: Preizkušanec za preizkus utrujenosti, model križno varjenega spoja konice rotorja rovokopača

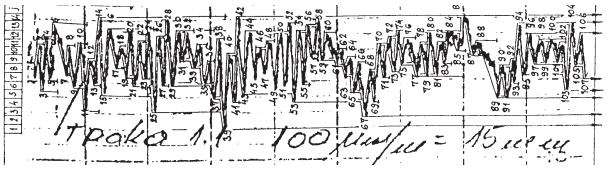

Figure 9: Stress variations measured in rotor excavator operation

Slika 9: Variacije napetosti, izmerjene pri delu rovokopača

The specimen for experimental fatigue testing was modelled as a critical cross-welded joint to simulate the bearing structure component exposed to cracking (**Figure 8**). The applied variable loading of the bearing structure consisted of transport (4 %), average operation (60 %) and full cut (36 %), as part of the digging process and by low-frequency self-vibrations. The time-dependent complex stresses of the structural elements are presented in **Figure 9**, as discriminated according to the stress origin in order to establish a stress spectrum simulating real-service loading [15]. The total spectrum of stress ranges also involved the pick loadings, representing 0.05 % to 10 % of the total operating time, which are so high that they can arrest the excavator operation. The experiments were performed at constant amplitude on a high-frequency resonant pulsator and by a defined spectrum on a servo-hydraulic closed-loop device. The obtained relations of stress, S, vs. the number of cycles, N, are presented in the double logarithmic diagram in **Figure 10**, designed as a F. S. for the constant amplitude loading ($S^{6.7}N$ = const), and as an A. S. for the simulating spectrum. The numerically obtained results for all the applied hypotheses are also presented for comparison.

The comparison of the fatigue testing results shows that the effect of the constant amplitude is more obvious (**Figure 10**), indicating that the structure in real operating conditions with a different amplitude can exhibit a longer fatigue life than expected, based on laboratory tests using a constant amplitude. The four hypotheses considered revealed a too optimistic fatigue

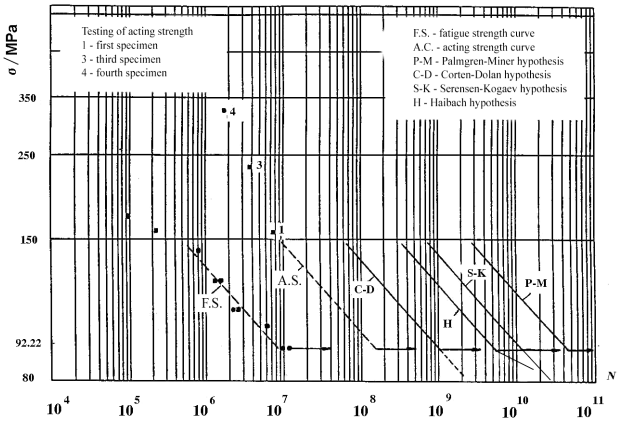

Figure 10: Comparison of *S–N* curves, obtained experimentally with constant (F. S.) and a variable amplitude loading spectrum (stress spectrum) (A. S.) and calculated by linear accumulation hypothesis (Corten-Dolan – C-D, Haibach – H, Serensen-Kogaev – S-K and Palmgren-Miner – P-M)

Slika 10: Primerjava eksperimentalnih odvisnosti *S-N* s konstantno (F. S.) in spremenljivo amplitudo spektra obremenitve (spekter napetosti) (A. S.) in izračunane s hipotezo linearne akumulacije (Corten – Dolan – C-D, Haibach – H, Serensen-Kogaev – S-K in Palmgren-Miner – P-M)

life compared to the experimental results, overestimating the number N_D for the fatigue limit. For this reason they should be applied with caution. It should be noted that the Haibach hypothesis is proposed for welded joints.

5 CONCLUSION

When applying the experimental results it is clear that the numerical models in the structural analysis have to be applied with a necessary caution because their efficiency is dependent on the considered influencing factors, since all the relevant factors and their real effect on the situation must be considered. It was found that in the case of a welded vessel exposed to internal pressure the applied model produces conservative – and thus acceptable – results, and that in the case of the fatigue of the rotor excavator's welded components the numerical model results overestimate the experimental values and cannot be applied as sufficiently conservative.

Acknowledgement

The paper is prepared with the financial support of the Serbian Ministry of Science and Environment Protection – project ON 14027 "Special topics in fracture mechanics of materials".

6 REFERENCES

[1] R. W. Nichols: The use of fracture mechanics as an engineering tool, The 1984 ICF Honour Lecture, ICF 6, New Delhi, India, 1984

[2] SINTAP: Structural Integrity Assessment Procedure, Final Report, EU-Project BE 95-1462. Brite Euram Programme, Brussels, 1999

[3] N. Gubeljak, U. Zerbst: SINTAP- **S**tructural **INT**egrity **A**ssessment **P**rocedure, in From fracture mechanics to structural integrity

assessment, ed. Z. Radaković and S. Sedmak, DIVK, TMF, Beograd, 2004

[4] F. M. Burdekin: The assessment of critical crack size in pressure vessels, the monograph Modern aspects of desing and manufacturing of pressure vessels and penstocks. ed. S. Sedmak, GOŠA, TMF, Beograd, 1982

[5] R. P. Reed, H. I. MacHenry, M. B. Kasen: A fracture mechanics evaluation of flaws in pipeline girth welds, Welding Research Council Bulletin, No 245, 1979

[6] B. Bozić, S. Sedmak, B. Petrovski, A. Sedmak: Crack gowth resistance of weldment constituents in a real structure, Bulletin T. Cl de l'Academie serbe des Sciences at des Arts, Classe des Sciences techniques, No 25, Beograd, 21–42, 1989

[7] M. M. Ratwani, F. Erdogan, G. R. Irwin: Fracture propagation in cylindrical shell containing an initial flaw, Lehigh University, Bethlehem, 1974

[8] ASTM E 1820-99: Standard Test Method for Measurement of Fracture Toughness

[9] D. T. Read: Experimental method for direct evaluation of the J contour integral, ASTM STP 791, 1983

[10] US-Yugoslav joint project Fracture mechanics of weldments, Annual reports, Faculty of Technology and Metallurgy, Beograd, Principal investicator S. Sedmak, 1982-1992

[11] M. A. Miner: Cumulative damage in fatigue, J. Appl. Mech. Trans. ASME, 12, 1945

[12] H. T. Corten, T. J. Dolan: Cumulative fatigue damage, Proc. Int. Conference on Fatigue of metals, ASME and IME, 1956

[13] S. V. Serensen, V. P. Kogaev, R. M. Snejderovic: Bearing capacity and calculation of machine elements resistance, in Russian, Mashinostroenie, Moskva, 1975

[14] E. Haibach: Modifizierte lineare Schädenakkumulationshypothese zur Berücksichtigung des Dauerfestigheitsabfals mit fortschreitender Schädigung, Laboratorium fur Betriebsfestigheit, TM, No 50/70, Darmstadt, 1970

[15] M. Arsić: Correlation between endurance limit and fatigue threshold of welded joints, Ph. D. thesis, in Serbian, Mechanical Engineering Faculty, Priština, 1995

UDK/UDC 539.4:691.54
Izvirni znanstveni članek/Original scientific article

ISSN 1580-2949
MTAEC9, 41(4)179(2007)

IZRAČUN PARAMETROV WEIBULLOVE PORAZDELITVE ZA OCENO UPOGIBNE TRDNOSTI VALOVITIH STREŠNIH PLOŠČ

COMPUTATION OF THE PARAMETERS OF THE WEIBULL DISTRIBUTION FOR ESTIMATING THE BENDING STRENGTH OF CORRUGATED ROOFING SHEETS

Milan Ambrožič[1], Krunoslav Vidovič[2]

[1]Institut "Jožef Stefan", Jamova 39, 1000 Ljubljana, Slovenija
[2]Esal, d. o. o. Anhovo, Vojkova 9, 5210 Deskle, Slovenija
milan.ambrozic@ijs.si

Prejem rokopisa – received: 2006-11-20; sprejem za objavo – accepted for publication: 2007-02-21

V članku je opisana uporaba Weibullove porazdelitve pri vrednotenju večkratnih meritev nekaterih mehanskih veličin valovitih strešnih plošč iz vlaknocementa, ki so bile izdelane v redni proizvodnji podjetja Esal, d. o. o. Anhovo. Tu se omejimo na zlomno silo pri prečni upogibni obremenitvi plošče in zlomni moment pri vzdolžni upogibni obremenitvi. V vsakem primeru smo izračunali oba Weibullova parametra, od katerih je pomemben predvsem Weibullov modul, ki podaja širino porazdelitvene funkcije merjene veličine.

Ključne besede: vlaknocementi, valovite strešne plošče, mehanske lastnosti, Weibullova statistika

In this paper the application of the Weibull distribution for the evaluation of repeated measurements of some mechanical quantities on corrugated roofing sheets made from fibre-cement composites in the serial production of the company Esal d.o.o. Anhovo is described. The focus is on the breaking force in the transversal bending, loading and breaking moment during the longitudinal bending loading of the plate. For all cases the two Weibull parameters were calculated; especially important is the Weibull modulus, which gives the width of the distribution function of the measured quantity.

Key words: fibre-cement composites, corrugated roofing sheets, mechanical properties, Weibull statistics

1 UVOD

Vlaknocementi (VC) so kompoziti iz cementa in ojačitvenih vlaken, ki povečajo natezno in upogibno trdnost materiala; znano je namreč, da sam hidratizirani cement zdrži veliko večje tlačne obremenitve kot natezne. Zaradi nevarnosti za zdravje so azbestna vlakna v VC nadomestili z drugimi: z naravnimi (npr. lesno celulozo iz drevesnih vrst, ki so razširjene na področju uporabe vlaknocementnih izdelkov) in sintetičnimi (steklenimi, ogljikovimi, polivinilalkoholnimi itd.).[1-6] Od sintetičnih organskih vlaken so med najustreznejšimi tista iz polivinil alkohola (PVA). V podjetju Esal, d. o. o., v Anhovem, ki je mešana družba Salonita Anhovo in Eternita iz Švice, uporabljajo PVA-vlakna za izdelavo vlaknocementov za valovitne strešne plošče. Glede na število celih valov v plošči, 5 ali 8, označujemo plošče na kratko V5 ali V8. Pri razvoju novih VC gradbenih elementov in tudi med velikoserijsko proizvodnjo je treba s standardnimi preizkusi preveriti različne mehanske lastnosti materiala in izdelkov, tudi glede na namenskost in na klimatske razmere okolja, kjer naj bi izdelke vgrajevali[7-9].

Veliko je proizvodnih parametrov, s katerimi lahko izboljšamo kakovost vlaknocementnih izdelkov[5,10-13]. Kar se tiče samih ojačitvenih vlaken v cementni matrici, so pomembni vrsta, volumenski delež, dolžina in poravnanost vlaken[5]. Pri izbiri vrste vlaken je treba med drugim upoštevati njihov elastični modul, natezno trdnost in površinske lastnosti, ki omogočajo dober spoj med vlakni in cementno matrico. Poleg optimalnih mehanskih lastnosti izdelkov je treba gledati tudi na proizvodne stroške, saj so sintetična vlakna relativno draga. Tako je najugodnejši volumenski delež PVA-vlaken nekaj odstotkov.

Izmerjene vrednosti značilnih mehanskih lastnosti končnih izdelkov, npr. zlomne sile, navadno ustrezajo Weibullovi porazdelitvi, posebno pri krhkih materialih, kot sta keramika in cement[14-19]. Weibullovo porazdelitev so uspešno uporabili na številnih področjih, npr. v strojništvu, gradbeništvu, pri inženirski keramiki in biokeramiki[20-24]. Navadno se uporablja 2-parametrična Weibullova porazdelitev, ki bo podrobneje opisana v nadaljevanju, v nekaterih primerih pa je ustreznejša uporaba 3-parametrične Weibullove porazdelitve.

Pri vsaki seriji izdelanih plošč izmerimo v Esal-u nekatere mehanske lastnosti na nekaj vzorčnih ploščah, to je navadno od 12 do 15 preizkusnih plošč na teden. Tako se je nabralo že veliko število meritev in v tem prispevku bomo spoznali, da se dajo izmerjene mehanske količine na ploščah dobro opisati z 2-parametrično Weibullovo porazdelitvijo. Opisana bo koristnost uporabe Weibullove porazdelitve pri napovedi mehanskih

lastnosti izdelkov v velikoserijski proizvodnji. Za inženirja in za uporabnika vlaknocementnih izdelkov so Weibullovi diagrami nazoren prikaz statistične porazdelitve vrednosti merjene veličine in s tem mehanske zanesljivosti vlaknocementnih izdelkov.

2 SESTAVA IN DIMENZIJE VALOVITIH STREŠNIH PLOŠČ V5

O sestavi in izdelavi vlaknocementnih izdelkov po Hatzschekovemu postopku je v tej reviji že bil objavljen prispevek[11].Tu omenimo le, da so vhodne surovine za izdelavo strešnih plošč portlandski cement, voda, polnila in vlakna. Poleg ojačitvenih PVA-vlaken se uporabljajo tudi celulozna vlakna, med drugim zaradi olajšanja proizvodnega postopka. Skupni masni delež celuloznih in PVA-vlaken v navadni redni proizvodnji strešnih plošč je 6,1 % glede na trdne sestavine (brez vode in zraka); od tega je 1/3 masnega deleža PVA-vlaken in 2/3 celuloznih vlaken. Pri opisu dimenzij se omejimo na plošče V5, ki jih v Esalu izdelajo več kot plošč V8. Geometrijo plošč V5 določajo parametri: širina W = 920 mm, dolžina L = 1250 mm, valovna dolžina profila λ = 177 mm, višina profila (dvojna amplituda vala) H = 51 mm, debelina $T \approx 6$ mm.

3 MERJENJE MEHANSKIH LASTNOSTI PREIZKUSNIH PLOŠČ

Neposredno pred mehanskimi preskusi se plošče namakajo 24 h v vodi. S tem simuliramo slabše vremenske razmere; po namakanju se namreč poslabšajo mehanske lastnosti plošč.

Izmerili smo različne mehanske lastnosti plošč V5, od katerih v tem prispevku opišemo le zlomno silo pri prečni upogibni obremenitvi (glede na valove plošč, **slika 1a**) in zlomni moment pri vzdolžni obremenitvi (**slika 1b**). Za merjenje zlomne sile smo uporabljali laboratorijsko merilno napravo BP-10, Walter+Bai AG, Švica, ki ima merilno območje od 2 kN do 10 kN. Glede eksperimentalnih pogojev, kot so geometrijski parametri, smo upoštevali standarda EN 494[25] in DIN 274/1[26]. Razdalje na **sliki 1a** so podane v milimetrih. Naprava neposredno izmeri silo F_T pri prečnem (transverzalnem) zlomu, medtem ko zlomni moment M_L pri vzdolžnem (longitudinalnem) zlomu izračunamo iz zlomne sile F_L in geometrijskih parametrov:

$$M_L = \frac{F_L L_s}{4L} \qquad (1)$$

kjer je L_s razmik med sredinama podpor, L pa dolžina plošče. Enota za moment je sicer N m, vendar pa računamo zlomni moment na dolžinsko enoto plošče; da poudarimo to renormalizacijo zlomnega momenta, bomo zanj pisali enoto N m/m. Relativne napake pri meritvah so približno 0,5 % za silo in 0,1 % ali manj za

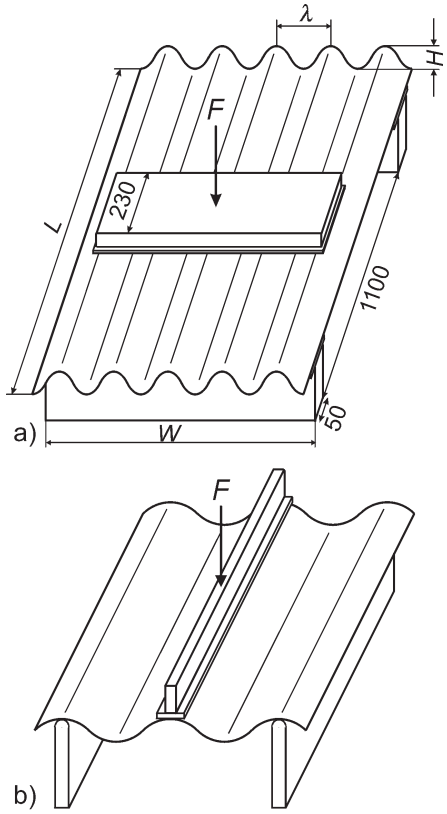

Slika 1: Geometrija pri prečni (a) in vzdolžni (b) upogibni obremenitvi plošče V5 glede na evropska standarda EN 494 in DIN 274/1

Figure 1: Geometry for transversal (a) and longitudinal (b) bending loading of the plate V5, in agreement with the European standards EN 494 and DIN 274/1

dolžinske dimenzije. Zato lahko iz enačbe (1) ocenimo še relativno napako za zlomni moment, to je 0,7 %.

Omenimo še, da lahko pri obeh načinih upogibne obremenitve izračunamo tudi druge veličine, npr. efektivno upogibno trdnost materiala. Zaradi valovite geometrije plošč je treba upogibne trdnosti računati numerično, in merilna naprava je povezana z računalnikom, ki ima ustrezni računalniški program.

4 STATISTIČNA OBDELAVA PODATKOV

Velikokrat se pri statistični obravnavi izmerjenih ali izračunanih podatkov zadovoljimo z izračunom povprečne vrednosti in standardne deviacije veličine, ki pa nam ne povesta vse informacije o statistični porazdelitvi vrednosti merjene veličine. Zato je priporočljivo najprej ugotoviti (če je to mogoče!), za katero statistično porazdelitveno funkcijo v danem primeru sploh gre, potem pa najti proste parametre te funkcije. Čeprav se verjetno v večini primerov pri statistični obravnavi za večje množine podatkov uporabi Gaussova porazdelitev, je za nekatere mehanske lastnosti konstrukcijskih materialov (kovine, keramika, cement in beton) ustreznejša Weibullova porazdelitev.

Označimo merjeno veličino z x. Njeno porazdelitev lahko opišemo s katerokoli od naslednjih dveh funkcij. Prva je navadna porazdelitvena funkcija ali verjetnostna gostota $p(x)$, tako da pomeni njen določeni integral

$$P(a \le x \le b) = \int_a^b p(x)\mathrm{d}x \qquad (2a)$$

verjetnost, da bo izmerjena vrednost veličine x ležala med vrednostima a in b. Druga funkcija je kumulativna porazdelitvena funkcija

$$P(x) = \int_{x_{\min}}^{x} p(x')\mathrm{d}x' \qquad (2b)$$

ki pomeni verjetnost, da bo izmerjena vrednost dane veličine ležala med teoretično najmanjšo možno vrednostjo $x_{\min}$ in variabilno vrednostjo x.

Tako sta 2-parametrični Weibullovi porazdelitveni funkciji naslednji:

$$p(x) = \frac{m}{x_0}\left(\frac{x}{x_0}\right)^{m-1} \exp\left(-\left(\frac{x}{x_0}\right)^m\right) \qquad (3a)$$

$$P(x) = 1 - \exp\left(-\left(\frac{x}{x_0}\right)^m\right) \qquad (3b)$$

Weibullova parametra sta Weibullov modul m in umeritveni parameter x_0 (angleško scale parameter). Parameter x_0 v literaturi imenujejo tudi karakteristični parameter: če je merjena veličina x na primer sila F, potem ta parameter označimo z F_0 in ga imenujemo karakteristična sila. Weibullov modul je brezdimenzijski in je za značilne krhke snovi veliko večji od 1, karakteristični parameter pa ima dimenzijo spremenljivke x. Oba parametra določata širino krivulje $p(x)$: čim večji je m in čim manjši x_0, tem ožja je krivulja, hkrati x_0 podaja tudi pričakovano vrednost spremenljivke x (enačbi 5). Čeprav funkciji $p(x)$ in $P(x)$ dajeta ekvivalentno informacijo o statistični porazdelitvi, je za relativno majhno število izmerjenih vrednosti spremenljivke x primernejša direktna uporaba funkcije $P(x)$. Funkcijo $P(x)$ bomo na kratko imenovali Weibullova funkcija. Njeni mejni vrednosti sta $P(0) = 0$ in $P(\infty) = 1$, pri čemer je teoretično najmanjša možna vrednost veličine x kar enaka nič. Omenimo še, da dobimo 3-parametrično Weibullovo statistiko iz 2-parametrične tako, da dodamo še parameter premika $x_{\min}$ in v desnih straneh enačb (3) naredimo transformacijo $x \rightarrow x - x_{\min}$; to pomeni, da je teoretično najmanjša možna vrednost veličine x enaka $x_{\min}$ namesto nič. **Sliki 2** prikazujeta 2-parametrično Weibullovo funkcijo za $m = 10$ v naravni skali in v skali, kjer je graf linearizirani. Sliki ponazorita tudi geometrijski pomen obeh parametrov: Weibullov modul m je smerni koeficient premice v linearizirani grafu, pri $x = x_0$ pa je verjetnost P enaka $1 - 1/e \approx 63{,}2$ %, temu pa ustreza točka (0, 0) v linearizirani grafu (krožca na obeh slikah).

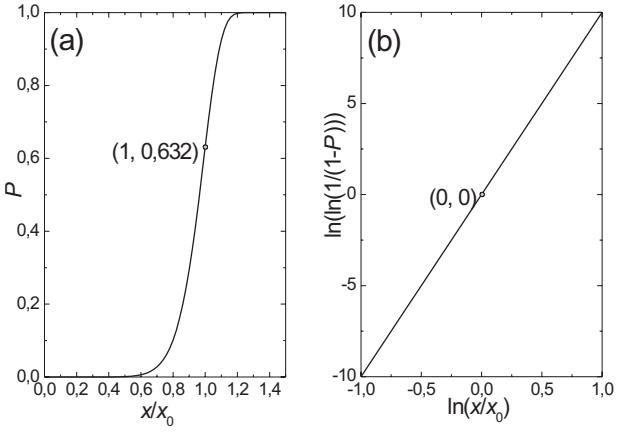

Slika 2: Graf funkcije $P(x/x_0)$ za $m = 10$; a) naravni spremenljivki, b) linearizirani graf s prirejenima spremenljivkama. Območje neodvisne spremenljivke v grafu (b) ustreza intervalu x/x_0 od $1/e$ do e, v mejnih točkah pa je verjetnost P praktično 0 in 1.

Figure 2: Diagram of the function $P(x/x_0)$ for $m = 10$; a) natural variables, b) linear diagram with transformed variables. The range of the independent variable in diagram (b) corresponds to the interval x/x_0 from $1/e$ from e, while the probability P is practically 0 and 1, respectively, for these limit points.

Pri danem statističnem vzorcu imamo N izmerjenih ali izračunanih vrednosti spremenljivke x, ki jih označimo z x_i. Cilj je najti Weibullova parametra, ki najbolj ustrezata statističnemu vzorcu[16,27-32]. Vrednosti x_i najprej uredimo po velikosti od najmanjše do največje. Nato vsakemu (i-temu po vrsti) izmerku priredimo še ocenjeno verjetnost P_i; za kar obstaja več načinov, največkrat pa se uporablja preprosta enačba:

$$P_i = \frac{i - 0{,}3}{N + 0{,}4} \qquad (4)$$

Tako dobimo N urejenih parov (x_i, P_i), ki jim priredimo Weibullovo funkcijo, tako da se jim najbolj prilega. Pri tem si pomagamo z linearizacijo enačbe (3b), kot prikazuje **slika 2b**. Povleči moramo premico, ki se najbolj prilega množici točk v transformiranem kordinatnem sistemu. Namesto prikaza na **sliki 2b** raje uporabljamo posebne Weibullove diagrame z originalnima spremenljivkama in nelinearno skalo, kot je prikazano na **sliki 3**.[16]

Ko sta Weibullova parametra znana, lahko izračunamo različne statistične veličine, kot sta pričakovana vrednost $\langle x \rangle$ in standardna deviacija σ_x veličine x:

$$\langle x \rangle = x_0 \cdot \Gamma\left(1 + \frac{1}{m}\right) \qquad (5a)$$

$$s_x = x_0 \cdot \sqrt{\Gamma\left(1 + \frac{2}{m}\right) - \Gamma^2\left(1 + \frac{1}{m}\right)} \qquad (5b)$$

kjer je Γ gama funkcija.

Ker sklepamo o statistični verjetnosti iz omejenega števila podatkov, sta izračunana parametra m in x_0 pravzaprav le oceni in ne natančni teoretični vrednosti, pa čeprav bi bila sama porazdelitev res natančno

Weibullova.[27] Zato navadno podajamo interval 90 % zaupanja (na kratko 90 % IZ); npr. če je za parameter m ta interval enak 90 % IZ = 8–12, to pomeni, da lahko pričakujemo z verjetnostjo 90 %, da je prava vrednost m res med 8 in 12.

5 REZULTATI IN RAZPRAVA

Kot zgled vzemimo izmerjene vrednosti F_T in M_L za nebarvane plošče V5 z zgoraj navedenimi merami iz redne proizvodnje v letih 2003 in 2004, kar nam da okrog 400 meritev za obe leti skupaj za vsako mehansko veličino. Vrednosti smo ovrednotili z Weibullovo statistiko, kjer je spremeljivka x sila F_T ali moment M_L. Rezultate za N = 50, 100, 200 in 400 podatkov za obe veličini prikazujeta tabeli 1 in 2; pri tem za prve tri vrednosti N vzamemo po vrsti podatke iz leta 2003, za N = 400 pa podatke obeh let. Po standardu EN 494 naj bi se sicer sila F_T preračunala na 1 m širine plošče, vendar je zaradi nazornosti v **tabeli 1** prikazana izmerjena sila za dejansko širino 920 mm; preračun za širino 1 m bi nam dal nekaj večje vrednosti, kot so v tabeli. Weibullov modul m je v vseh primerih reda velikosti 10, kar je značilno za krhke konstrukcijske materiale, kot so keramika in cementni kompoziti. Korelacijski koeficient ρ v zadnjem stolpcu tabele pove, kako dobro se Weibullova funkcija prilega eksperimentalnim podatkom; pri tem ρ = 1 pomeni popolno ujemanje. Zaradi večje nazornosti je v tabeli zapisan v odstotkih. Ugotavljamo, da je ρ v vseh primerih nad 96 %, torej Weibullova porazdelitev zelo dobro opisuje podatke. Poleg ocenjenih vrednosti Weibullovega modula m in parametra F_{T0} ali M_{L0}, ki ustreza parametru x_0 v enačbah (3), prikazujeta tabeli tudi ustrezne 90-odstotne intervale zaupanja. Intervali zaupanja za m so za N = 50 dokaj široki, ker je to še vedno premajhen vzorec za zares zanesljivo statistiko. Z naraščajočim N se vsi intervali zaupanja postopoma ožajo, in za m je 90 % IZ okrog desetine ocenjene vrednosti m šele pri N = 400. Za preizkus smo z uporabo naključnega generiranja števil izvedli tudi numerično simulacijo Weibullove porazdelitve za dan par parametrov m in x_0 in izračunane „naključne" vrednosti x_i statistično obdelali podobno, kot da bi bili eksperimentalni izmerki. Ugotovili smo podobno ožanje 90 % IZ za m in x_0 kot pri obdelavi pravih eksperimentalnih podatkov. V tabelah sta podane tudi ocene za pričakovano vrednost (PV) in standardno deviacijo (SD) veličin, izračunane iz enačb (5); te vrednosti so blizu vrednostim, dobljenimi s standardnimi statističnimi obrazci, npr.:

$$< x >= \frac{1}{N} \sum_{i=1}^{N} x_i$$

Tako kot za oba Weibullova parametra lahko izračunamo tudi 90%IZ za PV in SD zlomne sile in momenta, vendar jih tu ne navajamo. **Sliki 3** prikazujeta prilagoditev Weibullovih diagramov v nelinearni skali eksperimentalnim podatkom (N = 50) za zlomno silo in moment pri obeh načinih obremenitve. Narejeni sta bili s komercialnim programom za Weibullovo porazdelitev Reliasoft's Weibull ++.[16] Čim večja je strmina premice, tem ožja je statistična porazdelitev in manjša je verjetnost, da bodo v vsakdanji rabi izdelki odpovedali pri relativno majhnih mehanskih obremenitvah. Pri znanih Weibullovih parametrih lahko s preureditvijo enačbe (3b) izračunamo, kolikšna je pri podani verjetnosti, npr. P = 10 %, mejna vrednost veličine (sile ali momenta), tako da pričakujemo z verjetnostjo P, da bo meritev količine dala vrednost, manjšo od mejne vrednosti. Nekaj zgledov je prikazanih v **tabeli 3** za Weibullova parametra, ki ustrezata **tabelama 1 in 2** pri N = 400. **Tabelo 3** je treba pravilno razumeti: na primer, podatek za mejno silo 3518 N pri verjetnosti 0,1 %

Tabela 1: Parametri Weibullove porazdelitve za prečno zlomno silo F_T
Table 1: Weibull parameters for the transversal breaking force F_T

N	m		F_{T0}/N		PV, SD/N		ρ/%
	ocena	90 % IZ	ocena	90 % IZ	$<F_T>$	σ_{FT}	
50	11,63	9,86–13,72	6625	6475–6778	6341	661	97,0
100	12,71	11,40–14,16	6452	6355–6551	6196	594	97,5
200	11,70	10,83–12,65	6167	6093–6242	5904	612	96,7
400	12,29	11,63–12,98	6172	6124–6219	5919	586	98,3

Tabela 2: Parametri Weibullove statistike za vzdolžni zlomni moment M_L
Table 2: Weibull parameters for the longitudinal breaking moment M_L

N	m		M_{L0}/ (N·m/m)		PV, SD/(N·m/m)		ρ/%
	ocena	90 % IZ	ocena	90 % IZ	$<M_L>$	σ_{ML}	
50	10,74	8,90–12,95	99,81	97,57–102,10	95,23	10,71	99,0
100	11,32	9,93–12,89	98,52	97,01–100,05	94,20	10,08	98,6
200	11,04	10,11–12,06	96,54	95,44–97,65	92,22	10,10	98,6
400	11,21	10,57–11,88	97,75	96,96–98,55	93,43	10,09	98,7

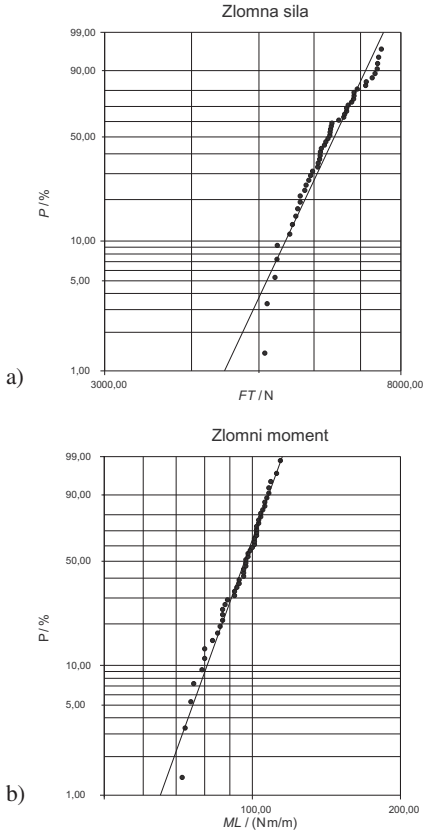

Slika 3: Weibullova grafa $P(F_T)$ (a) in $P(M_L)$ (b) za $N = 50$ meritev
Figure 3: Weibull diagrams $P(F_T)$ (a) and $P(M_L)$ (b) for $N = 50$ measurements

pomeni, da pričakujemo, da bo počila komaj ena od tisoč plošč pri prečni sili manj kot 3518 N.

Tabela 3: Mejne vrednosti zlomne sile in zlomnega momenta pri dani verjetnosti
Table 3: Limiting values of the breaking force and breaking moment for a given probability

P/(%	F_T /N	M_L/(N·m/m)
10	5139	79,97
1	4245	64,85
0,1	3518	52,79

6 SKLEP

Dvoparametrična Weibullova funkcija dobro opisuje porazdelitev zlomnih sil in momentov pri prečni in vzdolžni upogibni obremenitvi valovitih strešnih plošč V5 iz vlaknocementa. Vizualizacija podatkov z grafi (**sliki 3**) daje nazoren prikaz ujemanja med meritvami in Weibullovo porazdelitvijo. Čim večja je strmina premice, kar pomeni večji Weibullov modul m, tem večja je mehanska zanesljivost izdelkov, tj. manjša je verjetnost (pri istem parametru x_0), da se bodo plošče zlomile pri majhnih obremenitvah. To je posledica dejstva, da pomeni večji Weibullov modul manjše nihanje zlomnih obremenitev – manjšo standardno deviacijo. Ugotovitev ponazorimo z nekaj številkami. Vzemimo zaokroženo vrednost karakteristične zlomne sile F_0 = 6000 N, Weibullov modul pa naj bo 10 ali 15. Vrednost m ne vpliva bistveno na povprečno zlomno silo $\langle F_0 \rangle$: ta je enaka 5708 N pri m = 10 in 5794 N pri m = 15. Močno pa se spremeni verjetnostna porazdelitev za manjše sile. Za zgled vzemimo mejno silo 4000 N: pri m = 10 je verjetnost, da se izdelek zlomi pri manjši sili od dane vrednosti 4000 N, enaka 1,72 %, pri m = 15 pa je ta verjetnost samo še 0,23 %.

Pri oceni statističnih parametrov se moramo zavedati, da se lahko ta ocena zelo odmika od dejanske vrednosti parametrov. Iz **tabel 1 in 2** je razvidno, da je za 400 podatkov pričakovani interval (z 90-odstotnim zaupanjem) za resnično vrednost Weibullovega modula širok okrog 10 % izračunane vrednosti tega parametra, medtem ko je izračun drugega parametra Weibullove porazdelitve (F_{T0} ali M_{L0}) zanesljivejši.

7 LITERATURA

[1] J. B. Studinka, Asbestos substitution in the fibre cement industry. The International Journal of Cement Composites and Lightweight Concrete, 11 (**1989**), 73–78

[2] H. Savastano, P. G. Warden, R. S. P. Coutts, Potential of alternative fibre cements as building materials for developing areas, Cem. Concr. Compos., 25 (**2003**), 585–592

[3] R. S. P. Coutts, A review of Australian research into natural fibre cement composites, Cem. Concr. Compos., 27 (**2005**), 518–526

[4] V. Agopyan, H. Savastano, V. M. John, M. A. Cincotto, Developments on vegetable fibre-cement based materials in Sao Paolo, Brasil: an overview, Cem. Concr. Compos. 27 (**2005**), 527–536

[5] Y. P. Ma, B. R. Zhu, M. H. Tan, Properties of ceramic fiber reinforced cement composites, Cem. Conc. Res., 32 (**2005**), 296–300

[6] A. Peled, B. Mobasher, Pultruded fabric-cement composites, ACI Mater. J., 102 (**2005**), 15–23

[7] S. A. S. Akers, J. B. Studinka, Ageing behaviour of cellulose fibre cement composites in natural weathering and accelerated tests, The International Journal of Cement Composites and Lightweight Concrete, 11 (**1989**), 93–97

[8] S. A. S. Akers, Micromechanical studies of fresh and weathered fibre cement composites, The International Journal of Cement Composites and Lightweight Concrete, 11 (**1989**), 117–131

[9] P. Purnell, J. Beddows, Durability and simulated ageing of new matrix glass fibre reinforced concrete, Cem. Concr. Compos., 27 (**2005**), 875–884

[10] K. Vidovič, B. Lovreček, M. Hraste, Influence of surface charge on sedimentation and filtration behaviour of fibrous material, Chem. Biochem. Eng. Q, 10 (**1996**), 33–38

[11] K. Vidovič, Vlaknocement – Lastnosti materiala in tehnologija proizvodnje, Mater. tehnol. 38 (**2004**), 197–203

[12] C. Negro, A. Blanco, I. S. Pio, J. Tijero, Methodology for flocculant selection in fibre-cement manufacture, Cem. Concr. Compos., 28 (**2006**), 90–96

[13] Beaudoin JJ. Handbook of Fiber-Reinforced Concrete – Principles, Properties, Developments and Applications. Noyes Publications, New Jersey, US, 1990

[14] Weibull W. A statistical representation of fatigue failure in solids. Transactions of the Royal Institute of Technology 1949, No. 27, Stockholm

[15] Weibull W. A statistical distribution function of wide applicability. J Appl Mech. 18(**1951**), 293–297

[16] ReliaSoft's Weibull ++, Life Data Analysis Reference. ReliaSoft Publishing, 1992

[17] Kosmač T, Oblak C, Jevnikar P, Funduk N, Marion L. The effect of surface grinding and sandblasting on flexural strength and reliability of Y-TZP zirconia ceramic. Dental Mater. 15 (**1999**), 426–433

[18] Setien VJ, Armstrong SR, Wefel JS. Interfacial fracture tougness between resin-modified glass ionomer and dentin using three different surface treatment. Dent Mater. 21 (**2005**) 6, 498–504

[19] Lewis G, van Hooy-Corstjens CSJ, Bhattaram A, Koole LH. Influence of the radiopacifier in an acrylic bone cement on its mechanical, thermal, and physical propertires: Barium sulfate-containing cement versus iodine-containing cement. J. Biomed Mater Res B; 73B (**2005**) 1, 77–87

[20] Anton N, Ruiz-Prieto JM, Velasco F, Torralba JM. Mechanical properties and wear behaviour of ceramic matrix composites based on clinker portland doped with magnesia. J Mater Processing Tech; 78 (**1998**), 12–17

[21] Toutanji HA. Evaluation of the tensile strength of cement-based advanced composite wrapped specimens. Comp Sci Tech; 59 (**1999**) 15, 2261–2268

[22] Caliskan S. Aggregate/mortar interface: influence of silica fume at the micro- and macro-level. Cem Concr Compos; 25 (**2003**) 4–5, 557–564

[23] Li QS, Fang JQ, Liu DK, Tang J. Failure probability prediction of concrete components. Cem Concr Res; 33 (**2003**) 10, 1631–1636

[24] Huang JS, Cheng CK. Fracture toughness variability of foamed alumina cements. Cem Concr Res; 34 (**2004**) 5, 883–888

[25] EN 494, Fibre-cement profiled sheets and fittings for roofing – Product specification and test methods. December 2004

[26] DIN 274/1, Asbestzement-Wellplatten – Masse, Anforderungen, Prufungen. April 1972

[27] Quinn G. Flexure strength of advanced structural ceramics: A round robin. J. Am Ceram Soc; 73 (**1990**) 8, 2374–2384

[28] Ritter JE, Bandyopadhyyay N, Jakus K. Statistical reproducibility of dynamic and static fatigue experiments. Ceram Bullet; 60 (**1981**), 798–806

[29] Johnson LG. The median ranks of sample values in their population with an application to certain fatigue studies. Industrial Mathematics 1951; 2

[30] Lloyd DK, Lipow M. Reliability: Management, Methods and Mathematics. Prentice Hall, Englewood Cliffs, New Jersey,1962

[31] Li GQ, Cao H, Li QS, Huo D. Theory and its Application of Structural Dynamic Reliability. Earthquake Press, Beijing 1993

[32] Wu D, Zhou J, Li Y. Unbiased estimation of Weibull parameters with the linear regression method. J Eur Ceram Soc; 26 (**2006**), 1099–1105

UDC/UDK 669.041:669.14
Professional article/Strokovni članek

ISSN 1580-2949
MTAEC9, 41(4)185(2007)

INVESTIGATION OF THE INFLUENCE OF THE MELT SLAG REGIME IN A LADLE FURNACE ON THE CLEANLINESS OF THE STEEL

RAZISKAVA VPLIVA REŽIMA ŽLINDRE V PONOVČNI PEČI NA ČISTOST JEKLA

Zdeněk Adolf, Ivo Husar, Petr Suchánek

VŠB-Technical University of Ostrava, Department of Metallurgy, 17. listopadu 15/2172, Ostrava-Poruba, 708 33, Czech Republic
zdenek.adolf@vsb.cz

Prejem rokopisa – received: 2006-10-16; sprejem za objavo – accepted for publication: 2007-01-15

An experimental investigation of the influence of the ladle slag's chemical composition, the ladle slag's mass and the furnace slag's mass (during the tapping flow in the ladle) on the sulphur content in steel was carried out. The parameters of the slag and the steel were obtained in operational conditions of oxygen LD converter melts and from the subsequent ladle furnace LF processing.

Key words: ladle furnace, steel processing, effect of slag composition, refining effect

Eksperimentalna raziskava vpliva kemične sestave, količine (pri izlivu jekla v ponovco) na vsebnost žvepla v jeklu. Parametri jekla in žlindre so določeni pri izdelavi jekla v kisikovem konvertorju in obdelavi taline v ponovčni peči.

Ključne besede: ponovčna peč, procesiranje jekla, sestava žlindre, rafinacijski učinek

1 INTRODUCTION

Steel refined in a ladle furnace should have the following characteristics prior to casting:

- a chemical composition within the prescribed interval of alloying-element content and limited amounts of impurities,
- the required metallographic purity in terms of composition, magnitude, number and density of inclusions,
- the required casting temperature, depending on the steel's liquidus temperature.

In order to achieve these parameters the steelmaker usually has at his or her disposal a reheating ladle furnace, aluminium wire and a cored wire feeder, the mixing of steel with argon blowing or with induction stirring and an oxygen activity measurement system.

The slag is the most important factor for ensuring the quality of molten steel in the ladle. Ladle slag is formed from the products of de-oxidation of the steel, the added mixtures and from the corrosion products of the ladle lining, particularly at the slag line. Admixtures added intentionally to the slag ensure the required chemical composition of the slag, its fluidity and its ability to refine steel, i.e., for the absorption of inclusions and unwanted elements from the steel. The admixtures consist mostly of lime, fluorspar, calcium carbide and fireclay. Also, synthetic slags usually containing Al_2O_3, CaO, MgO, SiO_2, and a minimum of iron oxides, MnO and sulphur are used more and more often. Slags are often prepared from waste materials, either by simple mixing or by sintering, while the most expensive slags of the highest quality are manufactured by re-melting the input raw materials. These slags are usually used as a replacement for fluorspar and for the preservation of the required fluidity and for obtaining a sufficient refining effect in the ladle.

In this article the slag regime in a ladle furnace during steel refining, partly under fluorspar and partly under alumina slags, is compared. The slag regime of heats was evaluated with respect to the type and mass of the additions to the ladle, the ladle slag mass, the mass of converter slag overflowed to the ladle, the mass of corroded ladle lining and the slag desulphurisation capacity.

2 CHARACTERISTICS OF THE HEATS

The investigated steel I (intended for rail production) has an increased content of carbon (0.70–0.76 %), manganese (0.85–0.85 %) and silicon (0.30–0.40 %), controlled amounts of sulphur (0.01–0.02 %) and limited amounts of aluminium (0.003 %). It is, therefore, produced according to a technology without the use of aluminium and the deoxidation of steel in the ladle with coke, FeSi and MnSi. At the same time, during the tapping from the LD converter slag-forming materials are added to the ladle, e.g., lime (1200 kg), fluorspar (300 kg) and fireclay (150 kg), or lime, fluorspar and synthetic slag CCA with high contents of Al_2O_3 (see **Table 1**).

Table 1: Chemical composition of the synthetic slag CCA
Tabela 1: Kemična sestava sintetične žlindre CCA

w/%	Al_2O_3	CaO	MgO	SiO_2	S	Granularity
average	55.05	26.60	6.56	3.21	0.0295	5–50 mm
min	53.60	26.10	6.21	3.21	0.0290	
max	56.50	27.10	6.91	3.21	0.0300	

The refining of the rail steel was compared to that of the structural steel II with 0.18–0.20 % C, 0.41–0.51 % Mn, 0.20–0.30 % Si, with limited sulphur content (0.020 %) and a specified aluminium content (0.015–0.030 %). During tapping to the ladle this steel is deoxidised by aluminium and alloyed with FeMn and FeSi. At the same time, lime (1200 kg) and fluorspar (200 kg), or lime (900 kg) and synthetic slag CCA (700 kg), replacing the fluorspar, are added to the ladle.

The average chemical composition of ladle slags based on lime and fluorspar prior to the exit from the LF stand is given in **Table 2**.

Alumina slags were formed during the making of steel I for rails with synthetic slag CCA (700 kg) with 800 kg of lime (variant A), or with 600 kg of lime (variant B), and during the making of structural steel II with the synthetic slag CCA (700 kg) with 900 kg of lime. **Table 3** gives their average chemical compositions.

The average content of FeO in the fluorspar slags was 0.55 %, and in the alumina slags it was 2.0 %. If we compare both types of slags, then fluorspar slags have approximately 8 % to 11 % more CaO, higher basicity and a significantly higher content of CaF_2, which is added to the ladle during tapping in the form of fluorspar. On the other hand, alumina slags have higher contents of Al_2O_3 (by 9 % to 13 %) and MgO (by 1.5 % to 3.5 %). The synthetic slag CCA is, apart from converter slag and lime, also a source of MgO and Al_2O_3.

3 RESULTS AND DISCUSSION

The mass of the slag in the ladle was calculated from the balance of CaF_2 (Steel I - fluorspar slags) and from the balance of Al_2O_3 (Steel I and II - alumina slags). The mass of converter slag that overflowed into the ladle was calculated from the balance of CaO, and the extent of the wear of the ladle from the balance of MgO in the ladle slag. These data are for fluorspar slags and for two variants of alumina slags (rail steel I or structural steel II) summarised in **Table 4**.

The data in **Table 4** shows that ladle slags differ primarily in terms of their mass. Steel I fluorspar slags are formed, apart from SiO_2, from deoxidising silicon, lime, fluorspar and fireclay. The sum of the masses of these three components in the charge was approximately 1720 kg. The converter slag that overflowed into the ladle during the tapping affects the mass and the

Table 2: Chemical composition of the fluorspar slags (CaF_2)
Tabela 2: Kemična sestava fluoridnih (CaF_2) žlinder

w/%	CaO	SiO_2	Al_2O_3	MgO	CaF_2	S	Basicity
Steel I - rails							
average	52.9	23.5	4.2	4.9	13.29	0.64	2.25
min	50.9	21.9	3.5	4.5	11.74	0.42	2.12
max	55.2	25.2	5.1	5.7	14.48	0.75	2.52
Steel II - structural							
average	56.41	19.34	12.94	7.02	4.22	0.41	2.92
min	50.30	17.40	10.90	5.30	2.84	0.28	2.52
max	59.80	21.70	14.60	14.00	6.11	0.66	3.23

Table 3: Chemical compositions of alumina slags (CCA)
Tabela 3: Kemična sestava aluminatnih žlinder (CCA)

w/%	CaO	SiO_2	Al_2O_3	MgO	CaF_2	S	Basicity
Steel I - rails							
Variant A							
average	45.2	22.3	15.4	8.11	1.0	0.23	2.02
min	45.0	20.9	15.0	7.88	0.6	0.19	1.93
max	45.5	23.6	15.7	8.50	1.8	0.20	2.15
Variant B							
average	44.7	20.1	17.9	8.5	0.9	0.23	2.22
min	44.0	18.9	17.4	7.7	0.2	0.14	2.13
max	45.3	21.3	18.3	9.3	1.5	0.31	2.44
Steel II - structural							
average	45.23	17.89	22.05	8.51	0.10	0.20	2.53
min	41.10	15.50	18.00	6.80	0.00	0.13	2.12
max	48.30	21.10	25.30	11.00	0.27	0.31	2.95

Table 4: Parameters of ladle slags
Tabela 4: Parametri ponovčne žlindre

m/kg	LS	CS	MgO lining
Steel I - rails			
Fluorspar slags			
average	2411	325	71.5
min	2319	291	52.6
max	2508	380	82.9
Alumina slags – variant A			
average	2569	564	99.1
min	2519	431	93.4
max	2637	745	111.0
Alumina slags – variant B			
average	2210	590	69.0
min	2161	521	64.9
max	2273	719	75.6
Steel II – structural			
Fluorspar slags			
average	3374	1495	88.4
min	2632	153	57.3
max	4092	2800	99.8
Alumina slags			
average	3650	1693	86.9
min	2743	323	59.3
max	4645	3308	101.0

Note:
mass LS = mass of ladle slag, *m*/kg
mass CS = mass of converter slag that overflowed into the ladle, *m*/kg
MgO lining = wear of ladle lining, *m*/kg

chemical composition of the ladle slag. The mass of the slag in the heats with fluorspar slag was approximately 250 kg lower than the average for heats with alumina slag, for which a slightly lower overall mass of ladle slag was used. Alumina slags are formed of lime and synthetic slag CCA with an average mass of 1510 kg in variant A, and 1310 kg in variant B (again, apart from the SiO_2 from the deoxidising silicon).

For steel II the fluorspar slags are formed, apart from SiO_2 and Al_2O_3, from deoxidising silicon and aluminium, of lime and fluorspar with a total mass of 1400 kg; for alumina slags fluorspar is replaced with the slag CCA and the new mass of lime and slag CCA is 1600 kg.

The wear of the lining is expressed as the mass of MgO released from the ladle wear into the slag. The smallest lining wear for steel I was observed in the variant B, while the greatest wear was observed for the variant A of alumina slag. This is apparently related to the considerable differences in the total mass of slag in the ladle. The fluorspar slag shows – contrary to expectations – on average a low wear of lining; however, with a large scatter of values of approximately 30 kg of MgO.

The mass of converter slag overflowed into the ladle was, for the structural steel, three to five times greater then for the steel I. The share of converter slag in approximately 35 % of the total slag mass in the ladle is the source of the relatively high content of MgO in the ladle slag. The wear of the lining is practically the same for both types of ladle slags, and it is more influenced by the slag's mass then by the slag's chemical composition.

The parameters of the steel II desulphurisation with fluorspar and alumina slags are given in **Table 5**.

Table 5: Parameters of steel II desulphurisation by fluorspar and alumina slags
Tabela 5: Parametri razžveplanja jekla II s fluoridno in z aluminatno žlindro

	c'_S	$w\,[S]_{BOF}$/%	$w\,[S]_{LF}$/%	η/%	L_S
Fluorspar slag					
average	0.009945	0.026	0.011	68.769	40.24
min	0.006744	0.016	0.006	47.619	15.56
max	0.015171	0.043	0.018	80.000	55.00
Alumina slag					
average	0.002481	0.030	0.019	36.131	11.42
min	0.001426	0.018	0.011	20.000	4.48
max	0.003582	0.038	0.029	52.778	20.71

Note:
c'_S= sulphide capacity of slag, [1]
$[S]_{BOF}$ = sulphur content in steel during tapping from the converter, *w*/%
$[S]_{LF}$ = sulphur content in steel after treatment in the ladle furnace, *w*/%
η = rate of steel desulphurisation after treatment in the ladle furnace, %
L_S = distributing coefficient of sulphur (S_{slag} /S_{steel}), [1]

It can be concluded from Table 5 that fluorspar slags have a greater desulphurisation effect than alumina slags (see η, L_S), due to their higher basicity and their higher value of sulphide capacity given by the CaO content, which is on average higher by 10 %.

It was observed that fluorspar slags had a greater fluidity than alumina slags. This means that a small content of CaF_2 (up to 5 %) in the fluorspar slag increases the fluidity of this slag in a wide range of chemical compositions, especially of the CaO content. In contrast to this, the liquidity of the alumina slags can only approach that of the fluorspar slags in a relatively narrow range of content of the more active oxides (CaO, Al_2O_3, SiO_2, MgO). It is necessary to increase the CaO content to at least 50 %, the Al_2O_3 content to 25–30 %, and preserve the SiO_2 content at the level of 15–20 % and the MgO content at the level of 7 % in order to increase the sulphide capacity of the alumina slag to the level of the fluorspar slag.

4 CONCLUSION

The slag regime of heats during the making of rail steel I with a limited content of aluminium, increased amounts of C, Mn and Si and with controlled amounts of sulphur and structural steel II deoxidised by aluminium with a limited sulphur content are compared. The original fluorspar slag with low amounts of Al_2O_3 was substituted with an alumina slag in which the fluorspar was replaced by synthetic slag CCA.

The following conclusions from the comparison of both slag regimes of these heats (based on 200-tonne heats) are proposed:

a) Alumina slags formed by lime, synthetic slag CCA and the products of steel deoxidisation have a lower desulphurisation capacity then the fluorspar slags due to their lower CaO content.
b) The main advantage of fluorspar slags is in their great desulphurisation effect over a wide range of slag chemical compositions, even for a low CaF_2 content.
c) The liquidity of alumina slags is limited to a narrow range of CaO, Al_2O_3, SiO_2 and MgO content.
d) The mass of ladle slags is markedly affected by the volume of furnace slag overflowed into the ladle that has to be minimised.
e) The wear of the lining depends on the mass of the ladle slag. The effect of the slag's chemical composition is of minor importance.

This investigation was carried out in the frame of Grant project Reg. No. 106/04/0029 with the financial support of the Grant Agency of the Czech Republic and the project EUREKA Reg. No. OE214, with the financial support of the Ministry of Education, Youth and Sports of the Czech Republic.

UDC/UDK 553.61:663.3.041
Professional article/Strokovni članek

ISSN 1580-2949
MTAEC9, 41(4)189(2007)

THE INFLUENCE OF ILLITE-KAOLINITE CLAYS' MINERAL CONTENT ON THE PRODUCTS' SHRINKAGE DURING DRYING AND FIRING

VPLIV VSEBNOSTI GLIN ILINIT-KAOLINIT NA KRČENJE PRI SUŠENJU IN ŽGANJU

Milun Krgović[1], Nada Marstijepović[1], Mileta Ivanović[1], Radomir Zejak[2], Miloš Knežević[2], Snežana Đurković[1]

[1]University of Montenegro, Faculty of Metallurgy and Technology, Cetinjski put bb, 81000 Podgorica, Montenegro
[2]University of Montenegro, Faculty of Civil Engineering, Cetinjski put bb, 81000 Podgorica, Montenegro
milun@cg.ac.yu

Prejem rokopisa – received: 2007-01-19; sprejem za objavo – accepted for publication: 2007-03-18

In this paper an investigation of the influence of the mineral content of illite-kaolinite clays on the products' shrinkage during drying and firing is presented. Under the same conditions for preparing raw materials and ceramic mass, as well as under the same firing regime, the products' shrinkage during drying and firing is mostly influenced by the amounts of quartz and the illite and kaolinite clay minerals.

Keywords: clay, linear shrinkage, total shrinkage, sintering, porosity

Predstavljena je raziskava vpliva vsebnosti glin ilinit-kaolinit na krčenje pri sušenju in žganju. Pri enakih pogojih priprave surovega materiala in keramike in enakemu režimu žganja na krčenje najbolj vpliva razmerje med kremenom ter glino ilinit-kaolinit.

Ključne besede: glina, linearno krčenje, skupno krčenje, sintranje, poroznost

1 INTRODUCTION

The illite-kaolinite clays differ significantly in mineral composition from illite, kaolinite, quartz, feldspar, Fe_2O_3 and $CaCO_3$ [1,2]. The presented raw material composition, depending on the sintering temperature, produces solid-state reactions, polymorphic transformations of quartz and liquid-phase formation[3]. Besides the sintering temperature of the ceramic mass, the raw material mineral content also has an important role for the relations between the microstructure constituents[4]. The appearance of the liquid phase accelerates the solid-state reactions[5]. The mineral content of illite-kaolinite clays, besides other factors, determines the formation of new crystal phases during the sintering process, and the polymorphic transformations of quartz caused by volume changes[6].

During the drying of shaped ceramic products, the simultaneous transfer of mass and heat in the homogeneous polydispersive system material with water occurs[7]. The water is transported from the internal area of the material through capillaries to the surface of the products, where it evaporates. The process depends on the diffusion and evaporation rates. The difference in the water content on the surface and in the inside layers of the material enables humidity to transfer continuously from the inside to the surface by diffusion[8]. The volume changes during the drying induce internal stresses.

2 EXPERIMENTAL

Two types of illite-kaolinite clays were used for the preparation of samples (the clays are marked "PV" and "BP"). The samples were formed by plastic shaping in a mould of parallelepiped shape with dimensions 7.7 cm × 3.9 cm × 1.6 cm and marked with the numbers 1, 2, 3, 4, 5 … 15.

The clays' analyses consisted of a determination of the mineral content with x-ray analysis, as well as chemical and granulometric analyses with a determination of the particle size distribution. The grain shape was determined microscopically. The linear and volume shrinkage of the samples during the drying in air to a constant mass and during drying in a dryer at 110 °C were determined too.

The samples were fired at 800 °C, 900 °C, 1000 °C, 1100 °C and 1200 °C. The total porosity, the mineral content by x-ray analysis, and the microscopic analyses were assessed for the sintered samples.

3 RESULTS AND DISCUSSION

On the basis of the mineral and chemical compositions shown in **Figure 1**, **Figure 2** and **Table 1**, it was concluded that the investigated specimens were illite-kaolinite clay types containing α-quartz, carbonate and Fe_2O_3. In the "BP" clay the content of α-quartz was

Table 1: Chemical composition of clay
Tabela 1: Kemična sestava gline

Oxides	SiO_2	Fe_2O_3	Al_2O_3	CaO	MgO	Na_2O	K_2O	SO_3	Ig. loss
Clay "BP" Percentage by weight, *w*/%	72.68	5.70	10.98	0.48	0.70	0,31	1.12	–	8.03
Clay "PV" Percentage by weight, *w*/%	71	5.51	10.55	1.42	0.62	0.45	1.86	0.25	8.34

lower and there was a larger content of illite and kaolinite. The granulometric analysis shows a higher average content of "PV" clay grain (**Table 2**), although the pulverization of the clays was performed under the same conditions. This is due to the difference in mineral content, particularly the higher percentage of quartz in the "PV" clay.

The higher content of α-quartz in the "PV" clay and the higher average content of grains explain the lower average value of the volume shrinkage for the 15 samples during the air drying to a constant mass (**Figure 3, Figure 4 and Table 3**). The results of the volume shrinkage, as well as the average value for 15 samples during drying in a dryer to a constant mass, show higher values of the volume shrinkage for the samples based on "PV" clay (**Figure 5, Figure 6 and Table 4**). The higher the content of α-quartz, the lower the content of clay minerals and the higher average value of the grains in this clay enable the easier transport of water from the internal area of the samples through the capillaries to the surface at a drying temperature of 110 °C. The different values of the volume shrinkage of the samples during drying are the consequence of an unequal pressure during plastic shaping in a mould.

Table 2: Average grains value of the investigated clay types
Tabela 2: Povprečna velikost zrn v preiskanih glinah

Clay type	Average grains value (MV), *d*/μm
"BP"	17
"PV"	27

Table 3: Average values of volume shrinkage during drying in air to the constant mass
Tabela 3: Povprečno volumensko krčenje pri sušenju na zraku do konstantne mase

Clay type	Average values of volume shrinkage (for 15 samples) /%
"BP"	18.4
"PV"	15.8

Table 4: Average values of volume shrinkage during drying in dryer to the constant mass
Tabela 4: Povprečno volumensko krčenje pri sušenju v sušilniku do konstantne mase

Clay type	Average values of volume shrinkage (for 15 samples) /%
"BP"	0.98
"PV"	1.65

The volume shrinkage during firing is smaller for the samples based on the "PV" clay (**Figure 7**). The X-ray

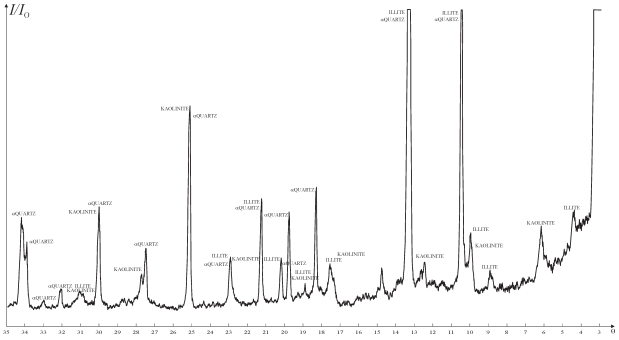

Figure 1: X-ray diffractogram of "PV" clay
Slika 1: Rentgenski difraktogram "PV"-gline

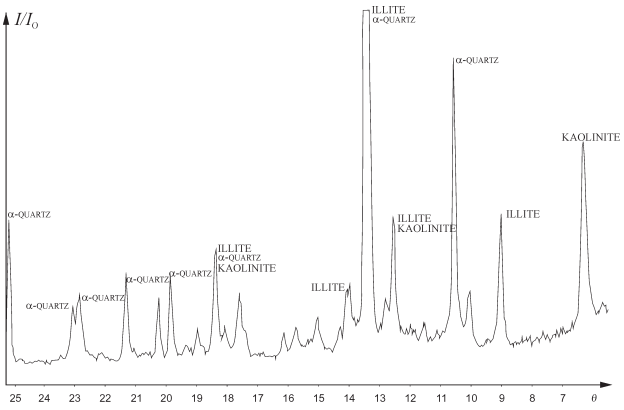

Figure 2: X-ray diffractogram of "BP" clay
Slika 2: Rentgenski difraktogram "BP"-gline

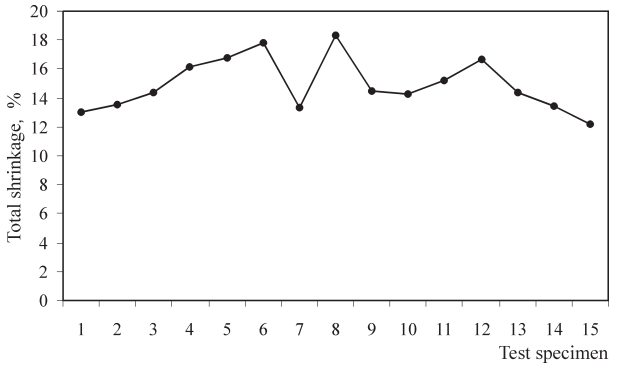

Figure 3: Volume shrinkage during drying to a constant mass in air ("PV" clay)
Slika 3: Volumensko krčenje pri sušenju do konstantne mase na zraku ("PV"-glina)

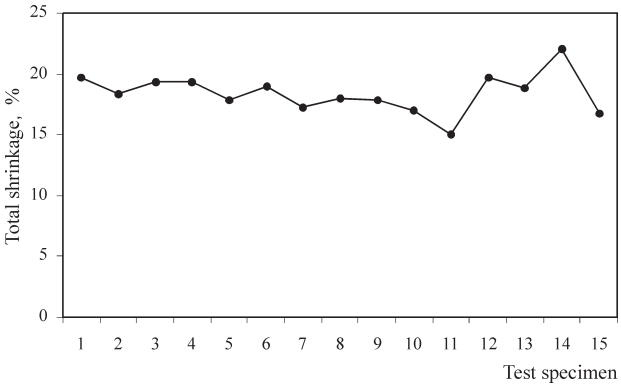

Figure 4: Volume shrinkage during drying to a constant mass in air ("BP" clay)
Slika 4: Volumensko krčenje pri sušenju do konstantne mase na zraku ("BP"-glina)

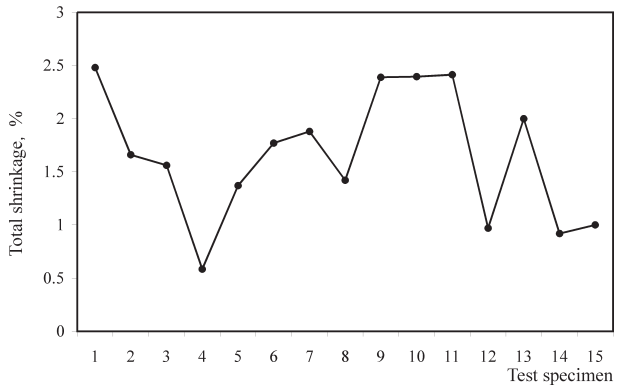

Figure 5: Volume shrinkage during drying to a constant mass in dryer ("PV" clay)
Slika 5: Volumensko krčenje pri sušenju do konstantne mase v sušilniku ("PV"-glina)

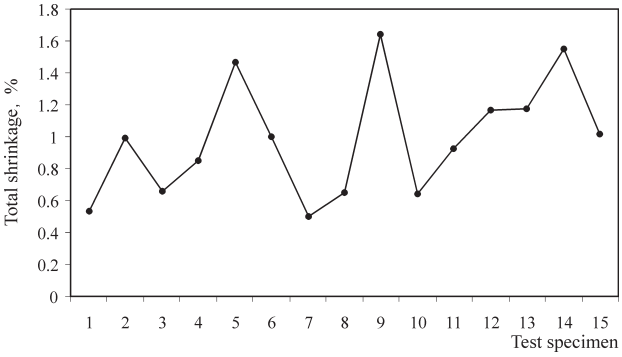

Figure 6: Volume shrinkage during drying to a constant mass in dryer ("BP" clay)
Slika 6: Volumensko krčenje pri sušenju do konstantne mase v sušilniku ("BP"-glina)

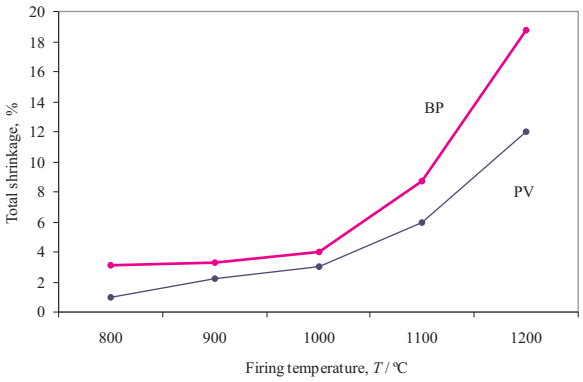

Figure 7: Volume shrinkage during sintering
Slika 7: Volumensko krčenje pri žganju

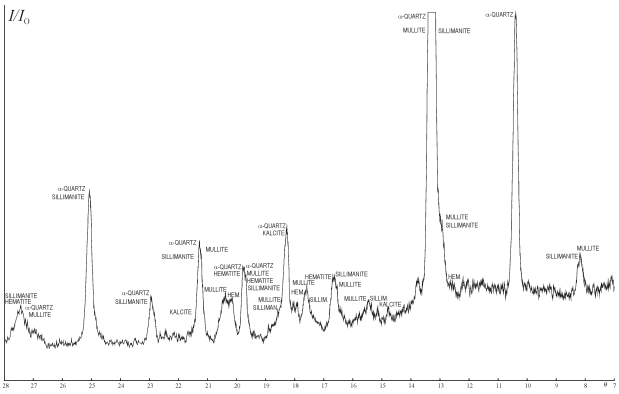

Figure 8: X-ray diffractogram of sintered product ("BP" clay, T = 1200 °C)
Slika 8: Rentgenski difraktogram za sintrani produkt ("BP"-glina, T = 1200 °C)

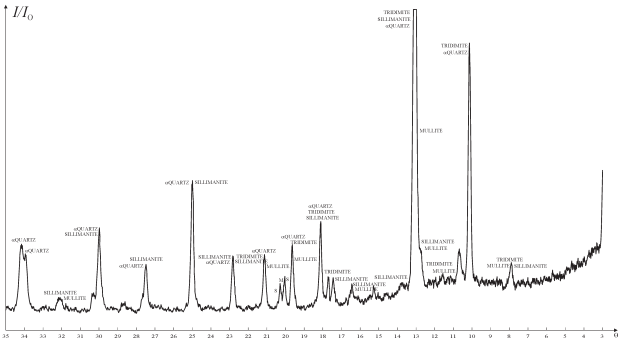

Figure 9: X-ray diffractogram of sintered product ("PV" clay, T = 1200 °C)
Slika 9: Rentgenski difraktogram za sintrani produkt ("PV"-glina, T = 1200 °C)

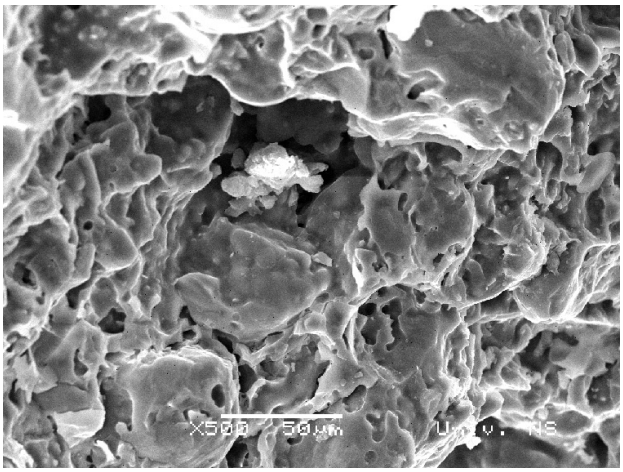

Figure 10: Microstructure of sintered product ("PV" clay, T = 1200 °C)

Slika10: Mikrostruktura sintranega produkta ("PV"-glina, T = 1200 °C)

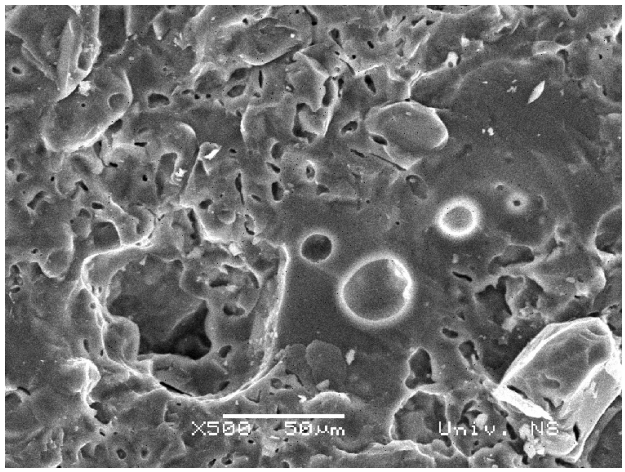

Figure 11: Microstructure of sintered product ("BP" clay, T = 1200 °C)

Slika 11: Mikrostruktura sintranega produkta ("BP"-glina, T = 1200 °C)

analysis of the sintered products shows a higher content of the minerals sillimanite, $Al_2O_3 \cdot SiO_2$, and mullite, $3Al_2O_3 \cdot 2SiO_2$, formed during the sintering of the samples based on "BP" clay (**Figure 8**). The higher content of the α-quartz in the "PV" clay and the higher total porosity explain the lower volume shrinkage during sintering, when the quartz is partly transformed into tridimite (**Figure 9**). The microstructures of the sintered products are shown in **Figures 10 and 11**.

4 CONCLUSION

The investigation of the influence of illite-kaolinite clays' mineral content on the linear and volume shrinkage during drying and firing shows that the shrinkage depends on the following factors:

- Using the same conditions for the preparation of raw materials and ceramic mass during drying in air and in a dryer to a constant mass, the most important factor is the influence of the relation between the quartz and clay's minerals content
- the values of the volume and linear shrinkage of samples during the firing process depend also on the relation between the quartz and the clay's minerals content. This influence is particularly strong at temperatures above 1000 °C.

5 REFERENCES

[1] M. Tecilazić-Stevanović, *Principles of Ceramic Technology*, Faculty of Technology and Metallurgy, University of Belgrade, Belgrade (1990)

[2] R. E. Grim, *Clay Mineralogy*, New York: McGraw-Hill Book Co., (1983)

[3] M. M. Krgović, N. Z. Blagojević, Ž. K. Jaćimović, R. Zejak, *Res. J. Chem. Environ.* 8 (**2004**) 4, 73–76

[4] J. Griffiths, *Ind. Min*., 272 (**1990**), 35–40

[5] M. M. Krgović, Z. K. Jaćimović, R. Zejak, *Tile & Brick Int*. 17 (**2001**) 3, 178–181

[6] M. Krgović, M. Ivanović, N. Z. Blagojević, Ž. Jaćimović, R. Zejak, M. Knežević, *Interceram,* 55 (**2006**) 2, 104–106

[7] Lj. Kostić-Gvozdenović, R. Ninković, *Inorganic Technology*, Faculty of Technology and Metallurgy, University of Belgrade, Belgrade (1997)

[8] B. Živanović, R. Vasić, O. Janjić, *Ceramic Tiles,* Institute of Materials in Serbia, Belgrade, (1985)

UDC/UDK 669.13:669.1(497.15)
Professional article/Strokovni članek

ISSN 1580-2949
MTAEC9, 41(4)193(2007)

THE APPLICATION OF SPHEROIDAL GRAPHITE CAST IRON IN BOSNIA AND HERZEGOVINA

UPORABA NODULARNE GRAFITNE LITINE V BOSNI IN HERCEGOVINI

Derviš Pihura, Mirsada Oruč

University of Zenica, Metallurgical institute "Kemal Kapetanović", Travnička cesta 7, 72000 Zenica, Bosnia and Herzegovina
pihura@yahoo.com

Prejem rokopisa – received: 2006-07-20; sprejem za objavo – accepted for publication: 2007-02-16

Modern technology ensures the quality and the economy of machine parts manufactured from spheroidal graphite iron (SGI) castings. Although this technology has been in widespread use in the EU countries for half a century and the production volumes continue to increase, in Bosnia and Herzegovina (B&H) there is no interest in the production and use of SGI. From an analysis of industrial facilities we have concluded that the foundry industry in B&H could also be competitive in the market for SGI.

Key words: Spheroidal graphite iron castings, machine parts

Moderna tehnologija zagotavlja kakovost in ekonomičnost strojnih delov, izdelanih iz nodularne grafitne litine. Čeprav je ta že pol stoletja veliko uporabljena v državah EU in v ZDA, obseg proizvodnje pa stalno raste, v Bosni ni zanimanja za proizvodnjo in uporabo nodularnih odlitkov. Iz analize industrijskih kapacitet sklepamo, da bi lahko bila livarska industrija v BiH konkurenčna tudi na trgu nodularnih odlitkov.

Ključne besede: nodularna siva litina, strojni deli

1 INTRODUCTION

Spheroidal graphite iron (SGI) castings are not produced and used in the metallurgical industry in Bosnia and Herzegovina (B&H), which is the opposite situation to most industrial countries, where the use of SGI castings increases at rates of up to 10 % per year (**Figure 1**). It is reasonable to expect that such industrial branches as energy, transport, agriculture, etc. will be forced into an increasing use of SGI, especially for moving and rotating machine parts, for example:

- The increasing speeds used on railways requires the substitution of some steel cast parts, for example, gears, with gears made from SGI. These gears are used to advantage when operating railways at speeds from a hundred up to a few hundred kilometres per hour.
- The automotive industry needs high-quality machine cast parts. The B&H foundry industry needs to set up for casting machine blocks from SGI, as well as other cast parts.
- The use of wind energy is a solution that B&H will soon exploit. When generating energy from wind machines, a great number of the parts are made from SGI.

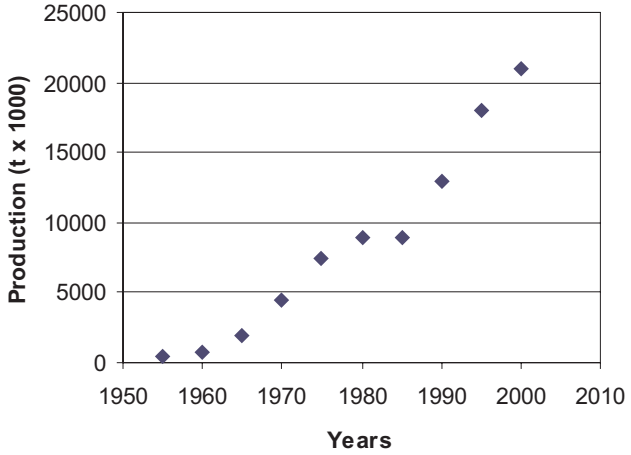

Figure 1: Growth in the world production of SGI from 1950 to 2000 [1]
Slika 1: Rast svetovne proizvodnje nodularnih odlitkov v obdobju 1950 do 2000 [1]

2 INVESTIGATIONS AND DEVELOPMENT OF SGI IN B&H

The development work for the production of parts from SGI castings began approximately 30 years ago at the "Kemal Kapetanovic" Metallurgical Institute in Zenica. The technology for the manufacture of specific SGI machine parts was developed at the institute, after which it was transferred to the former foundry of the Energoinvest company in Sarajevo, the foundry in Ilijaš, and other foundry companies.

The investigations were carried out to answer different questions, relating to:

- the economics of the production of SGI in B&H;
- the influence of properties due to the presence of residuals and impurities in the melting charge on the process of nodulation and the final degree of nodularity of the solidified SGI castings in relation to the extended and the conventional chemical analysis;

- the relation between the degree of nodularity and the microstructure homogeneity and the mechanical properties of SGI parts;
- the effect of the optimal addition of alloys and of the processing parameters on the nodulation;
- the kinetics of nodulation.

Many of the findings and the accumulated field experience could still be used for the renewal of the production of SGI and various castings [2,3], especially since customers may inquire about mutually exclusive properties for some specific castings.

3 CHARACTERISTICS OF SGI CASTINGS

It is clear that the production of castings from SGI of different quality levels could be revived in B&H in order to replace the supply or imports from abroad. In this way it is possible to produce castings from SGI for specific uses and for the substitution of steel castings. The melting temperature for SGI is about 300 °C lower than that for steel, and this in itself is a significant advantage in terms of saving energy and ecology. Apart from the better castability, the easier mechanical machining and the lower friction explain the continuous increase in the production of machine parts from SGI in the countries of the EU and the USA. It seems natural to expect that also in B&H SGI should again achieve the position it had in the foundry industry two decades ago, particularly since a large part of the production was delivered to customers abroad because of its high quality.

The increase in the world production of SGI (**Figure 1**) asks the question, which casting iron will dominate the production of castings: spheroidal or lamellar graphite iron, malleable cast iron or cast steel? Malleable cast-iron production started to decrease in the early 1980s, while SGI production increases continuously, partly because of the substitution of other cast irons and partly because of new uses for the castings. The increase in the production of SGI becomes clear from a comparison of the casting technology and the cast's properties in **Figure 2 and 3** [4]. The comparison accounts for several factors, such as, the chemical analysis, the mechanical properties, the section and size of the cast parts, the processing time, the assortment, the energy consumption, the total costs, the sampling, the testing and the examination and control [2].

The effect of graphite nodules on the stress-strain relations can be calculated from the equation

$$R_m = (1 - e^{-\alpha E_o - \varepsilon_t})/\alpha$$

where E_o is the modulus elasticity, α is a factor of the dependence of E_o from the stress up to the value of $R_{p0.2}$ and can be expressed as $\alpha = 1/R_{p0.2}$, and ε_t is the elongation.

The as-cast microstructures of SGI castings depend on the chemistry and the cooling rate. The microstructure consists of ferrite, pearlite and free carbides,

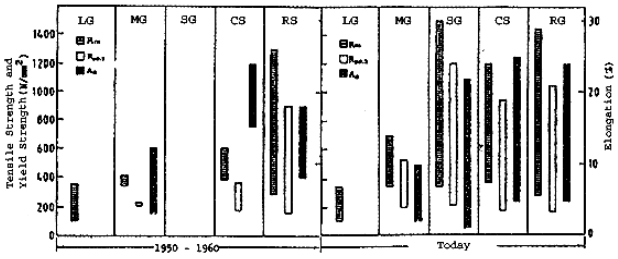

Figure 2: Mechanical properties of cast irons, cast steels and rolled steels for the period 1950–1960 (left-hand side) and 2000 (right-hand side) [2,5]; (LG – gray iron, MG – malleable iron, SG – spheroidal graphite iron, RS – rolled steel, CS – cast steel), (R_m – Tensile strength, $R_{p0.2}$ – Yield strength, A_5 – elongation)

Slika 2: Mehanske lastnosti železovih litin, litega železa in valjanega jekla za obdobje 1950–1960 (levo) in 2000 (desno) [2,5]; (LG – siva litina, MG – temprana litina, SG – nodularna litina, RS – valjano jeklo, CS – jeklena litina), (R_m – raztržna trdnost, $R_{p0.2}$ – meja plastičnosti, A_5 – raztezek)

and it can be modified by subsequent heat treatments. When compared to steel castings, SGI castings are less expensive, show a greater yield, and thus a greater weight of the final cast part versus the weight of the used melt. The consumption of energy for the production of SGI parts is one-third lower than that for cast steel parts. Also, the investment costs for the SG foundry are lower than those for a steel foundry [2,4].

The basic advantages of SGI are accurate dimensions, better uniformity of the strength properties, less hot and cold cracking, and an easy heat treatment. Additional advantages of the SGI castings are a lower coefficient of thermal expansion, less shrinkage and piping, better damping properties, better fluidity, better machinability and reduced surface scaling. Also, with SGI castings the effect of the wall thickness on the mechanical properties is smaller (2).

4 FURTHER DEVELOPMENT

The increasing market demand for a better and more uniform quality of castings and improved mechanical properties as well as the pressure to lower prices require that foundries develop and use improved technologies and new grades of castings. They have to do this even though the optimal combination of different properties can be obtained with SGI (**Figure 3**).

Accordingly, the world production of SGI is increasing rapidly; an increase of about 50 % was achieved in the past decade, a growth rate that is only rarely met with other major industrial products. However, methods for the production of parts competing for the same applications as SGI castings are also constantly improving and the SGI foundry industry is forced to compete, not only with other cast-iron alloys, but also other materials that are potential substitutes. In this competition SGI castings seem to be in better position than other iron castings because of the more

Properties	Cast Iron					
	Gray	Malleable	White	Steel	Nodular	
Fluidity						
Machining			NA			
Damping						
Surface hardening			NA			
Modulus off elasticity			NA			
Impact energy			NA			
Corrosion resistant						
Strength/Mass			NA			
Abrasion						
Costs						
The best						The worst

Figure 3: Properties of cast ferrous materials [5,6]
Slika 3: Lastnosti litih železnih materialov [5,6]

ecologically friendly production process and its lower costs.

With the introduction of new technological processes such as ADI and ESR better mechanical properties of SGI (**Figure 2 and 3**) are being achieved and the competitiveness of castings, especially for use in more severe conditions, is strengthened.

5 CONCLUSION

The overall competitiveness involving the economy of production and the properties make SGI castings very suited to a number of applications in machine parts. The increased production and use of SGI castings is justified if advanced technology and organisation are achieved in the production and delivery of castings with qualities that satisfy export-market requirements.

6 REFERENCES

[1] www.ductile.org/didata/Section 2/figures
[2] R. Hummer et al.: Giesserei, 88 (**2001**) 9–11, 49–55
[3] World Steel production, Worldsteel News, January (**2005**), 5
[4] F. Kritschtner: Livarski vestnik, (**1996**), 4, 1–15
[5] Gusseisen mit Kugelgraphite: Giesserei Kalender, 1985, 72–81
[6] P.M. Cabanne, Hommes & Fonderie, 306 (**2000**), Aout/Septembre, 18–22